

# Gravitational Lensing by Dark Matter Caustics

C. Charmousis<sup>a</sup>, V. Onemli<sup>b</sup>, Z. Qiu<sup>b</sup> and P. Sikivie<sup>b,c</sup>

<sup>a</sup>*LPT\**, Bât. 210, Université de Paris-Sud, F-91405 Orsay, France

<sup>b</sup>*Department of Physics, University of Florida, Gainesville, FL 32611-8440*

<sup>c</sup>*KITP, University of California, Santa Barbara, CA 93106-4030*

(November 29, 2018)

## Abstract

Dark matter caustics have specific density profiles and, therefore, precisely calculable gravitational lensing properties. We present a formalism which simplifies the relevant calculations, and apply it to four specific cases. In the first three, the line of sight is tangent to a smooth caustic surface. The curvature of the surface at the tangent point is positive, negative or zero. In the fourth case the line of sight passes near a cusp. For each we derive the map between the image and source planes. In some cases, a point source has multiple images and experiences infinite magnification when the images merge. Unfortunately, for the dark matter caustics expected in realistic galactic halo models, the angular resolution required to resolve the multiple images is not presently achievable. A more promising approach aims to observe the distortions caused by dark matter caustics in the images of extended sources such as radio jets.

PACS numbers: 95.35.+d

Typeset using REVTeX

---

\*Unité mixte du CNRS (UMR 8627).

## I. INTRODUCTION

Gravitational lensing techniques have proven useful in studying the distribution of dark matter in the universe. They have been used to reveal the existence of massive compact halo objects (MACHOs) in galaxies [1], and to constrain the mass distribution in galaxy clusters [2]. In this paper, we calculate the gravitational lensing properties of dark matter caustics [3–5]. Gravitational lensing by dark matter caustics has been discussed by Hogan [6]. We confirm Hogan’s results for the case he considered, called the ‘concave fold’ in our nomenclature. We study additional cases and introduce a formalism to facilitate the calculations.

In the cold dark matter (CDM) cosmology, caustics in the distribution of dark matter are plentiful once density perturbations enter the non-linear regime. A dark matter caustic is a surface in physical space where the dark matter density is large because the sheet on which the particles lie in phase-space has a fold there. Dark matter caustics can move about but they are stable.

To see the validity of the preceding statements, note that before the onset of galaxy formation the cold dark matter particles lie on a thin 3-dim. sheet in 6-dim. phase-space. The thickness of this sheet is the primordial velocity dispersion  $\delta v$  of the particles. It is of order [4]

$$\delta v_a(t) \sim 3 \cdot 10^{-17} \left( \frac{10^{-5} \text{eV}}{m_a} \right)^{5/6} \left( \frac{t_0}{t} \right)^{2/3} \quad (1.1)$$

for axions, and

$$\delta v_W(t) \sim 10^{-11} \left( \frac{\text{GeV}}{m_W} \right)^{1/2} \left( \frac{t_0}{t} \right)^{2/3} \quad (1.2)$$

for weakly interacting massive particles (WIMPs), such as the lightest supersymmetric particle in supersymmetric extensions of the Standard Model. In Eqs. (1.1-2),  $t_0$  is the present age of the universe and  $m_a$  and  $m_W$  are respectively the masses of the axion and WIMP. The present average axion number density is

$$n_a(t_0) = \frac{1.5 \cdot 10^{64}}{\text{pc}^3} \Omega_a \left( \frac{h}{0.7} \right)^2 \left( \frac{10^{-5} \text{eV}}{m_a} \right) \quad (1.3)$$

where  $\Omega_a$  is their present energy density in units of the critical density, and  $h$  is the Hubble expansion rate in units of 100 km/(s·Mpc). Likewise, for WIMPs

$$n_W(t_0) = \frac{1.5 \cdot 10^{50}}{\text{pc}^3} \Omega_W \left( \frac{h}{0.7} \right)^2 \left( \frac{\text{GeV}}{m_W} \right) \quad (1.4)$$

The large exponents in Eqs. (1.3-4) indicate that the density of cold dark matter particles is enormous in terms of astronomical length scales. Being effectively collisionless, the particles experience only gravitational forces. These are universal and vary only on huge distances compared to the interparticle distance. Hence the sheet on which the particles lie in phase-space is continuous. It cannot break and therefore its evolution is constrained by topology.

In contrast, in present numerical simulations of galactic halo formation, the particle mass  $m$  is of order  $10^6 M_\odot$  and hence the number density

$$n(t_0) = \frac{1.4 \cdot 10^{-13}}{\text{pc}^3} \Omega \left( \frac{h}{0.7} \right)^2 \left( \frac{10^6 M_\odot}{m} \right) . \quad (1.5)$$

The resolution of the simulations is inadequate to describe the dynamical evolution of the phase-space sheet and the physical implications of its existence.

Where a galaxy forms, the sheet wraps up in phase-space, turning clockwise in any two dim. cut  $(x, \dot{x})$  of that space.  $x$  is the physical space coordinate in an arbitrary direction and  $\dot{x}$  its associated velocity. The outcome of this process is a discrete set of flows at any physical point in a galactic halo [7]. Two flows are associated with particles falling through the galaxy for the first time ( $n = 1$ ), two other flows are associated with particles falling through the galaxy for the second time ( $n = 2$ ), and so on. Scattering in the gravitational wells of inhomogeneities in the galaxy (e.g. molecular clouds and globular clusters) are ineffective in thermalizing the flows with low values of  $n$ .

Caustics appear wherever the projection of the phase-space sheet onto physical space has a fold [3–5]. Generically, caustics are surfaces in physical space. They separate regions with differing number of flows. On one side of a caustic surface there are two more flows than on the other. Because caustic surfaces occur wherever the number of flows changes, they are topologically stable, in direct analogy with domain walls. At the caustic, the dark matter density is very large.

There are two types of caustics in the halos of galaxies, inner and outer. The outer caustics are simple fold ( $A_2$ ) catastrophes located on topological spheres surrounding the galaxy. They occur where a given outflow reaches its furthest distance from the galactic center before falling back in. The inner caustics are rings [3]. They are located near where the particles with the most angular momentum in a given inflow reach their distance of closest approach to the galactic center before going back out. A caustic ring is a closed tube whose cross-section is a  $D_{-4}$  (also called *elliptic umbilic*) catastrophe [4]. The existence of these caustics and their topological properties are independent of any assumptions of symmetry.

Dark matter caustics have very well defined density profiles, and hence calculable gravitational lensing signatures [6]. It is the purpose of this paper to derive these signatures in a number of specific cases. In the limit of zero velocity dispersion ( $\delta v = 0$ ), the density diverges when one approaches a caustic surface, on the side which has two extra flows, as the inverse square root of the distance to the surface. This divergence is cut off if there is velocity dispersion, because the location of the caustic surface gets smeared over some distance  $\delta x$ . For the dark matter caustics in galactic halos,  $\delta x$  and  $\delta v$  are related by [3]

$$\delta x \sim \frac{R \delta v}{v} \quad (1.6)$$

where  $v$  is the order of magnitude of the velocity of the particles in the flow and  $R$  is the distance scale over which that flow turns around, i.e. changes its direction. For a galaxy like our own,  $v = 500$  km/s and  $R = 200$  kpc are typical orders of magnitude.

As was mentioned earlier, the primordial velocity dispersion of the leading cold dark matter candidates is very small. Using Eqs. (1.1-2), one finds that axion caustics in galactic halos are typically smeared over

$$\delta x_a \sim 10^{10} \text{ cm} \left( \frac{10^{-5} \text{ eV}}{m_a} \right)^{5/6} \quad (1.7)$$

as a result of their primordial velocity dispersion, whereas WIMP caustics are smeared over

$$\delta x_W \sim 3 \cdot 10^{15} \text{ cm} \left( \frac{\text{GeV}}{m_W} \right)^{\frac{1}{2}} \quad (1.8)$$

It should be kept in mind, however, that a cold dark matter flow may have an effective velocity dispersion which is larger than its primordial velocity dispersion. Effective velocity dispersion occurs when the sheet on which the dark matter particles lie in phase-space is wrapped up on scales which are small compared to the galaxy as a whole. It is associated with the clumpiness of the dark matter falling onto the galaxy. The effective velocity dispersion of a flow may vary from point to point, taking larger values where more small scale structure has formed, and taking the minimum primordial value where no small scale structure has formed. For a coarse-grained observer, the dark matter caustic is smeared over  $\delta x$  given by Eq. (1.6) where  $\delta v$  is the effective velocity dispersion of the flow.

Little is known about the size of the effective velocity dispersion of dark matter flows in galactic halos. However, in ref. [8], a triangular feature in the IRAS map of the Milky Way was interpreted as the imprint upon baryonic matter of the caustic ring of dark matter nearest to us. The sharpness of the feature's edges implies an upper limit of 20 pc on the distance  $\delta x$  over which that caustic is smeared, and hence an upper limit of order 50 m/s on the effective velocity dispersion of the corresponding flow.

The gravitational lensing effects of a caustic surface are largest when the line of sight is near tangent to the surface because the contrast in column density is largest there. The effects depend on the curvature of the caustic surface at the tangent point in the direction of the line of sight: the smaller the curvature, the larger the effects. A caustic is an oriented surface because one side has two more flows than the other. We will consider three cases of gravitational lensing by a smooth caustic surface. In the first case, the line of sight is near tangent to a caustic surface which curves towards the side with two extra flows; see Fig. 4. We call such a surface 'concave'. In the second case, the surface is 'convex', i.e. it curves away from the side with two extra flows; see Fig. 6. In the third case, the caustic surface has zero curvature at the tangent point (the radius of curvature is infinite), but the tangent line is entirely outside the side with two extra flows.

Caustic surfaces may have cusps. The outer dark matter caustics of galactic halos are topological spheres, which have no cusps. But the inner dark matter caustics of galactic halos are closed tubes whose cross-section is a  $D_{-4}$  catastrophe; see Fig. 2. This cross-section has three cusps. We call it a 'tricusps'. The fourth case of gravitational lensing which we consider has line of sight near a cusp, and parallel to the plane of the cusp; see Fig. 9.

Gravitational lensing produces a map of an object surface onto an image surface. The magnification is the inverse of the Jacobian of this map. Because dark matter caustics have well defined density profiles, it is a neat mathematical exercise to calculate their gravitational lensing characteristics. The images of extended sources may show distortions that can be unambiguously attributed to lensing by dark matter caustics in the limit of perfect observations. We will see that in three of the cases considered, a point source can have multiple images. In those cases, when two images merge, the Jacobian of the map vanishes

and the magnification diverges. So, at least in theory, it seems that gravitational lensing is a very attractive tool for investigating dark matter caustics. Observation of the calculated lensing signatures would give direct evidence for caustics and CDM.

We have been particularly motivated by the possibility [6] that the observer might be able to distinguish between axions and WIMPs by determining the distance over which the caustics are smeared. The nearby caustic, whose position is revealed according to ref. [8] by a triangular feature in the IRAS map of the Milky Way plane, is only 1 kpc away from us in the direction of observation. By observing the gravitational lensing due to that caustic, one may be able to measure  $\delta x$  as small as  $10^{13}$  cm, assuming an angular resolution of  $3 \cdot 10^{-9}$  radians. If  $\delta x$  turned out to be that small, the WIMP dark matter hypothesis would be severely challenged; see Eq. (1.8). Unfortunately, as will be shown below, the gravitational lensing due to a caustic only a kpc away from us is too weak to be observed with present instruments. It is well known that gravitational lensing effects are proportional to  $\frac{D_L D_{LS}}{D_S}$  where  $D_S, D_L$  and  $D_{LS}$  are respectively the distances from the observer to the source, from the observer to the lens and from the lens to the source. We will see below that, for the gravitational lensing effects of dark matter caustics to be observable with present technology, the lenses and sources must be as far as possible, at the cosmological distances of order Gpc. Even then, the observation of such effects will be difficult. Unfortunately, at Gpc distances it is not possible to measure  $\delta x$  as small as Eqs. (1.7-8) with foreseeable technology. So it seems unlikely that one will be able to distinguish between dark matter candidates on the basis of the gravitational lensing characteristics of the caustics they form. Henceforth, unless otherwise stated, the velocity dispersion is set equal to zero.

The remainder of this paper is organized as follows. In section II, we describe the outer and inner caustics of dark matter in galactic halos. We provide estimates of their sizes and of the strengths of their density profiles, using the self-similar infall model of galactic halo formation. In section III, the general formalism of gravitational lensing is reviewed. We show how the calculations can be streamlined for the case of gravitational lensing by dark matter caustics. In section IV, we calculate the gravitational lensing properties of dark matter caustics in the four cases mentioned above. In section V, we summarize our conclusions.

## II. DENSITY PROFILES OF CAUSTICS

In this section we discuss the density profiles of the dark matter caustics present in galactic halos. We consider the outer caustics first.

### A. Outer caustics

Outer caustics are closed surfaces (topological spheres) near the  $(n + 1)$ th turn-around radii with  $n = 1, 2, 3, \dots$ . Indeed the number of flows changes by two there because of the fall back of the particles. There is no caustic associated with the first turn-around, see Fig. 1. The outer caustics are described by simple “fold” ( $A_2$ ) catastrophes. Their density profile is:

$$d_n(\sigma) = \frac{A_n}{\sqrt{\sigma}} \Theta(\sigma) \quad (2.1)$$

for small  $\sigma$ , where  $\sigma$  is the distance to the caustic,  $\Theta(\sigma)$  is the Heaviside function, and  $A_n$  is a constant which we call the *fold coefficient*.  $\sigma > 0$  on the side with two extra flows, i.e. towards the galactic center. Therefore, when an outer caustic is approached from the inside the density diverges as  $\sim \frac{1}{\sqrt{\sigma}}$ , abruptly falling to zero on the outside. The observation [9] of arc-like shells surrounding giant elliptical galaxies can be interpreted [10] as outer caustics in the distribution of baryonic matter falling onto those galaxies.

To estimate  $A_n$  in Eq. (2.1), consider the time evolution of CDM particles which are falling out of a galactic halo for the  $n$ th time and then fall back in. Let  $R_n$  be the turn-around radius. We assume that the rotation curve of the galaxy is flat near  $r = R_n$  with time-independent rotation velocity  $v_{\text{rot}}$ . The gravitational potential is then:

$$V(r) = v_{\text{rot}}^2 \ln \left( \frac{r}{R_n} \right) \quad . \quad (2.2)$$

The particles have trajectory  $r(t)$  such that

$$\left| \frac{dr}{dt} \right| = \sqrt{2(E - V(r))} = v_{\text{rot}} \sqrt{2 \ln \left( \frac{R_n}{r} \right)} \quad , \quad (2.3)$$

where  $E$  is the energy per unit mass. Eq. (2.3) neglects the angular momentum of the particles. This is a good approximation at turnaround since the particles are far from their distance of closest approach to the galactic center. Finally, we assume that the flow is stationary. In that case the number of particles flowing per unit solid angle and per unit time,  $\frac{dN}{d\Omega dt}$ , is independent of  $t$  and  $r$ , and the caustic is located exactly at the  $(n + 1)$ th turn-around radius  $R_n$ .

Let us emphasize that none of the assumptions - spherical symmetry, flat rotation curve, time independence of the gravitational potential, radial orbits, and stationarity of the flow - affect the existence of the outer caustics or the fact that they have the density profile given by Eq. (2.1). The assumptions are made only to obtain estimates of the coefficients  $A_n$ .

The mass density of particles,  $d_n(r)$ , follows from the equality:  $2 \frac{dN}{d\Omega dt} dt = \frac{d_n(r)}{m} r^2 dr$ , where  $m$  is the mass of each particle. The factor of 2 appears because there are two distinct flows, out and in. Using Eq. (2.3) we obtain the density distribution near the  $n$ th outer caustic:

$$d_n(r) = 2 \frac{dM}{d\Omega dt} \Big|_n \frac{1}{r^2 v_{\text{rot}} \sqrt{2 \ln \left( \frac{R_n}{r} \right)}} \quad , \quad (2.4)$$

where  $\frac{dM}{d\Omega dt} \equiv m \frac{dN}{d\Omega dt}$ . Near the caustic,  $\ln \left( \frac{R_n}{r} \right) = \frac{\sigma}{R_n}$  where  $\sigma = R_n - r$ . Inserting this into Eq. (2.4) and comparing with Eq. (2.1), we find:

$$A_n = \frac{\sqrt{2}}{v_{\text{rot}}} \frac{dM}{d\Omega dt} \Big|_n R_n^{-3/2} \quad . \quad (2.5)$$

Estimates of  $R_n$  and  $\frac{dM}{d\Omega dt} \Big|_n$  can be extracted from ref. [11] for the case of self-similar infall [12,13]. The infall is called *self-similar* if it is time-independent after all distances are

rescaled by the turn-around radius  $R(t)$  at time  $t$  and all masses are rescaled by the mass  $M(t)$  interior to  $R(t)$ . In the case of zero angular momentum and spherical symmetry, the infall is self-similar if the initial overdensity profile has the form  $\frac{\delta M_i}{M_i} = \left(\frac{M_0}{M_i}\right)^\epsilon$  where  $M_0$  and  $\epsilon$  are parameters [12]. In CDM theories of large scale structure formation,  $\epsilon$  is expected to be in the range 0.2 to 0.35 [11]. In that range, the galactic rotation curves predicted by the self-similar infall model are flat [12].

The  $R_n$  and  $\left.\frac{dM}{d\Omega dt}\right|_n$  do not depend sharply upon  $\epsilon$ . Our estimates are for  $\epsilon = 0.2$  because they can be most readily obtained from ref. [11] in that case. For  $\epsilon = 0.2$ , the radii of the  $(n + 1)$ th turn-around spheres are approximately

$$\{R_n : n = 1, 2, \dots\} \simeq (240, 120, 90, 70, 60, \dots) \text{ kpc} \cdot \left(\frac{v_{\text{rot}}}{220 \text{ km/s}}\right) \left(\frac{0.7}{h}\right) \quad . \quad (2.6)$$

Moreover, one has

$$\left.\frac{dM}{d\Omega dt}\right|_n \frac{1}{v_{\text{rot}}} = F_n \sqrt{2} \frac{v_{\text{rot}}^2}{4\pi G} \quad , \quad (2.7)$$

with

$$\{F_n : n = 1, 2, \dots\} \simeq (20, 8, 5, 4, 3, \dots) 10^{-2} \quad . \quad (2.8)$$

Combining Eqs. (2.5 - 2.8), we find

$$\begin{aligned} \{A_n : n = 1, 2, \dots\} \sim (2, 2, 2, 3, 3, \dots) \cdot \frac{10^{-5} \text{ gr}}{\text{cm}^2 \text{ kpc}^{1/2}} \\ \cdot \left(\frac{v_{\text{rot}}}{220 \text{ km/s}}\right)^{1/2} \left(\frac{h}{0.7}\right)^{3/2} \quad . \quad (2.9) \end{aligned}$$

Generally the outer caustics are 'concave', i.e. they are curved towards the side which has two extra flows. Their radius of curvature is of order  $R_n$ . The lensing by concave caustic surfaces is discussed in section IV.A.

In the next subsection, we discuss the density profiles of inner caustics.

## B. Inner caustics

The inner caustics [3] are closed tubes whose cross-section, shown in Fig. 2, is a  $D_{-4}$  catastrophe [4]. They are located near where the particles with the most angular momentum in a given inflow are at their distance of closest approach to the galactic center. We call them 'caustic rings'. For simplicity, we study caustic rings which are axially symmetric about the  $z$ -direction as well as reflection symmetric with respect to the  $z = 0$  plane. The dark matter flow is then effectively 2-dimensional. In galactocentric cylindrical coordinates, the flow at such a caustic ring is described by [4]:

$$z(\alpha, \tau) = b \alpha \tau \quad \text{and} \quad \rho(\alpha, \tau) = a + \frac{u}{2}(\tau - \tau_0)^2 - \frac{s}{2}\alpha^2 \quad , \quad (2.10)$$

to lowest order in an expansion in powers of  $\alpha$  and  $\tau$ .  $\alpha$  and  $\tau$  are parameters labeling the particles in the flow.  $\rho$  is distance to the  $z$ -axis.  $\tau$  is the time a particle crosses the  $z = 0$  plane.  $\alpha$  is the declination of the particle, relative to the  $z = 0$  plane, when it was at last turnaround.  $b$ ,  $a$ ,  $u$ ,  $\tau_0$  and  $s$  are constants characteristic of the caustic ring.  $b$ ,  $u$ ,  $s$  and  $a$  are positive, whereas  $\tau_0$  can have either sign.  $a$  is the radius of the ring; see Fig. 2. The transverse dimensions of the ring are  $p = \frac{1}{2}u\tau_0^2$  and  $q = \frac{\sqrt{27}}{4}\frac{b}{\sqrt{us}}p$  in the  $\hat{\rho}$  and  $\hat{z}$  directions respectively. The cross-section of the ring has three cusps. So we call it the “tricusp”. The cusps are topological properties of the caustic. Their presence does not depend on any assumptions of symmetry.

The physical space density is given by [4]

$$d(\rho, z) = \frac{1}{\rho} \sum_{j=1}^n \frac{dM}{d\Omega d\tau}(\alpha, \tau) \frac{\cos(\alpha)}{|D_2(\alpha, \tau)|} \Big|_{(\alpha_j(\rho, z), \tau_j(\rho, z))} , \quad (2.11)$$

where  $\frac{dM}{d\Omega d\tau} = \frac{dM}{2\pi \cos(\alpha) d\alpha d\tau}$  is the mass falling in per unit time and unit solid angle.  $\alpha_j(\rho, z)$  and  $\tau_j(\rho, z)$ , with  $j = 1, \dots, n$ , are the solutions of  $\rho(\alpha, \tau) = \rho$  and  $z(\alpha, \tau) = z$ .  $n(\rho, z)$  is the number of flows at  $(\rho, z)$ .  $n = 2$  outside the caustic tube, whereas  $n = 4$  inside.  $D_2(\alpha, \tau) \equiv \det \mathcal{D}(\alpha, \tau)$  with

$$\mathcal{D}(\alpha, \tau) \equiv \begin{pmatrix} \frac{\partial \rho}{\partial \alpha} & \frac{\partial z}{\partial \alpha} \\ \frac{\partial \rho}{\partial \tau} & \frac{\partial z}{\partial \tau} \end{pmatrix} = \begin{pmatrix} -s\alpha & b\tau \\ u(\tau - \tau_0) & b\alpha \end{pmatrix} \quad (2.12)$$

is the Jacobian of the map  $(\alpha, \tau) \rightarrow (\rho, z)$ .

In the limit of zero velocity dispersion, the density of dark matter particles is infinite at the location of caustic surfaces. Thus, the location of the caustic ring surface is obtained by demanding that

$$D_2(\alpha, \tau) = -b[u\tau(\tau - \tau_0) + s\alpha^2] = 0 \quad . \quad (2.13)$$

This implies

$$\alpha(\tau) = \pm \sqrt{\frac{u}{s}\tau(\tau_0 - \tau)} \quad (2.14)$$

with  $0 \leq \frac{\tau}{\tau_0} \leq 1$ , and hence [4]

$$\rho(\tau) = a + \frac{u}{2}(\tau - \tau_0)(2\tau - \tau_0) \quad , \quad z(\tau) = \pm b \sqrt{\frac{u}{s}\tau^3(\tau_0 - \tau)} \quad , \quad (2.15)$$

for the location of the tricuspid outline. Near the surface of a caustic ring, but away from the cusps, the density profile is that of a simple fold:  $d(\sigma) = \frac{A}{\sqrt{\sigma}}\Theta(\sigma)$ , with  $\sigma > 0$  inside the tricuspid. In the next three subsections we calculate the fold coefficient  $A$  and the principal curvature radii,  $R_1$  and  $R_2$ , at arbitrary points on the surface of a caustic ring, other than the cusps. As a warm-up, we start with a special point, marked by a star in Fig. 2. In the fourth subsection, we obtain the density profile near the cusps.



1. A sample point

As an example, we determine the fold coefficient  $A$  at  $(\rho, z) = (a, 0)$ ; see Fig. 2. Setting  $\alpha = z = 0$ ,  $\sigma = \rho - a = \frac{1}{2}u(\tau - \tau_0)^2$  and  $\tau \simeq \tau_0$ , we have

$$|D_2(\tau)| \simeq 2b\sqrt{p\sigma} \quad . \quad (2.16)$$

Including the factor 2 for in and out flows, Eq. (2.11) yields:

$$d(\sigma) = \frac{dM}{d\Omega dt} \frac{1}{ab} \frac{1}{\sqrt{p\sigma}} \quad . \quad (2.17)$$

Therefore,

$$A_0 = \frac{d^2 M}{d\Omega dt} \frac{1}{ab} \frac{1}{\sqrt{p}} \quad , \quad (2.18)$$

where the 0 subscript is to indicate that  $A$  is being evaluated at the sample point.

To obtain a numerical estimate for  $A_0$ , we again use the self-similar infall model [12,13,11] with  $\epsilon = 0.2$ . For the  $n$ th ring, we have [3]

$$\{a_n : n = 1, 2, \dots\} \simeq (39, 19.5, 13, 10, 8, \dots)\text{kpc} \cdot \left(\frac{j_{\max}}{0.27}\right) \left(\frac{0.7}{h}\right) \left(\frac{v_{\text{rot}}}{220 \text{ km/s}}\right) \quad , \quad (2.19)$$

where  $j_{\max}$  is a parameter, with a specific value for each halo, which is proportional to the amount of angular momentum that the dark matter particles have [11]. Also,

$$\left.\frac{d^2 M}{d\Omega dt}\right|_n = f_n v_n \frac{v_{\text{rot}}^2}{4\pi G} \quad , \quad (2.20)$$

where  $v_n$  is the velocity of the particles in the  $n$ th caustic ring, and the dimensionless coefficients  $f_n$  characterize the density of the  $n$ th in and out flow. In the self-similar model [3]

$$\{f_n : n = 1, 2, \dots\} \simeq (13, 5.5, 3.5, 2.5, 2, \dots) \cdot 10^{-2} \quad (2.21)$$

for  $\epsilon = 0.2$ . The  $f_n$  are like the  $F_n$  in Eq. (2.7), but they describe the  $n$ th in and out flow near the caustic ring whereas the  $F_n$  describe that flow near turnaround.

Combining Eqs. (2.18) and (2.20) we have

$$A_{0,n} = \frac{v_{\text{rot}}^2}{4\pi G} \frac{f_n}{a_n} \frac{v_n}{b_n} \frac{1}{\sqrt{p_n}} \quad . \quad (2.22)$$

It was shown in ref. [4] that  $b_n$  and  $v_n$  are of the same order of magnitude. Also, in ref. [8], ten rises in the rotation curve of the Milky Way were interpreted as the effect of caustic rings. In that case, the widths  $p_n$  of caustic rings are determined from the observed widths of the rises. Typically one finds  $p_n \sim 0.1 a_n$ . Using this and  $v_n \sim b_n$ , Eq. (2.22) yields the estimates

$$\{A_{0,n} : n = 1, 2, \dots\} \sim (3, 4, 4, 5, 5, \dots) \cdot \frac{10^{-4} \text{ gr}}{\text{cm}^2 \text{ kpc}^{1/2}} \cdot \left(\frac{0.27}{j_{\text{max}}}\right)^{3/2} \left(\frac{h}{0.7}\right)^{3/2} \left(\frac{v_{\text{rot}}}{220 \text{ km/s}}\right)^{1/2}. \quad (2.23)$$

At the point under consideration,  $(\rho, z) = (a, 0)$ , the surface of the caustic ring is convex for all lines of sight, i.e. all tangents at that point are on the side with two extra flows. If the line of sight is in the  $z = 0$  plane, the curvature radius is  $a$ . If the line of sight is perpendicular to the  $z = 0$  plane, the curvature radius is  $2\frac{b^2}{su}p$ . Lensing by a convex caustic surface is discussed in subsection IV.B.

To obtain the lensing properties of the caustic ring surface at an arbitrary point, we need the coefficient  $A$  and the curvature radii  $R_1$  and  $R_2$  at all locations. We derive these quantities in the next two subsections.

## 2. The fold coefficient everywhere

We choose an arbitrary point on the tricusp, i.e. on the surface of the caustic ring. Its parameters are  $(\alpha_1, \tau_1)$  with  $\alpha_1$  given in terms of  $\tau_1$  by Eq. (2.14). The physical coordinates  $(\rho_1, z_1)$  are given in terms of  $\tau_1$  by Eq. (2.15). We assume that the point is not at one of the three cusps. The latter are located at  $\tau_1 = 0$ , at  $\tau_1 = \frac{3}{4}\tau_0$  with  $\alpha_1 > 0$ , and at  $\tau_1 = \frac{3}{4}\tau_0$  with  $\alpha_1 < 0$ .

The vanishing of  $D_2(\tau_1)$  implies the existence of a zero eigenvector of the matrix

$$\mathcal{D}(\tau_1) = \begin{pmatrix} -s\alpha_1 & b\tau_1 \\ u(\tau_1 - \tau_0) & b\alpha_1 \end{pmatrix}. \quad (2.24)$$

Let us define  $\theta_1(\tau_1)$  such that

$$\mathcal{D}(\tau_1) \begin{pmatrix} \sin(\theta_1) \\ \cos(\theta_1) \end{pmatrix} = 0. \quad (2.25)$$

We have

$$\sin(\theta_1) = \frac{b\tau_1}{\sqrt{(b\tau_1)^2 + (s\alpha_1)^2}} \quad \text{and} \quad \cos(\theta_1) = \frac{s\alpha_1}{\sqrt{(b\tau_1)^2 + (s\alpha_1)^2}}. \quad (2.26)$$

We define new Cartesian coordinates  $(\sigma, \eta)$  related to  $(\rho - \rho_1, z - z_1)$  by a rotation of angle  $\theta_1 + \frac{\pi}{2}$ :

$$\begin{pmatrix} \sigma \\ \eta \end{pmatrix} = \begin{pmatrix} -\sin(\theta_1) & -\cos(\theta_1) \\ \cos(\theta_1) & -\sin(\theta_1) \end{pmatrix} \begin{pmatrix} \rho - \rho_1 \\ z - z_1 \end{pmatrix}. \quad (2.27)$$

We now show that  $\sigma$  is the coordinate in the direction orthogonal to the caustic surface at  $(\rho_1, z_1)$ .

Consider small deviations about  $(\alpha_1, \tau_1)$  in parameter space:  $(\alpha, \tau) = (\alpha_1 + \Delta\alpha, \tau_1 + \Delta\tau)$ . Eq. (2.12) implies,

$$\begin{pmatrix} \Delta\rho \\ \Delta z \end{pmatrix} = \mathcal{D}^T(\tau_1) \begin{pmatrix} \Delta\alpha \\ \Delta\tau \end{pmatrix} + O(\Delta\alpha^2, \Delta\tau^2, \Delta\alpha\Delta\tau) \quad , \quad (2.28)$$

where  $T$  indicates transposition. The expansion of  $\sigma$  in powers of  $\Delta\alpha$  and  $\Delta\tau$  yields:

$$\sigma = O(\Delta\alpha^2, \Delta\tau^2, \Delta\alpha\Delta\tau) \quad , \quad (2.29)$$

because the first order terms vanish:

$$\left. \frac{\partial\sigma}{\partial\alpha} \right|_{(\alpha_1, \tau_1)} \Delta\alpha + \left. \frac{\partial\sigma}{\partial\tau} \right|_{(\alpha_1, \tau_1)} \Delta\tau = -(\Delta\alpha \quad \Delta\tau) \mathcal{D}(\tau_1) \begin{pmatrix} \sin(\theta_1) \\ \cos(\theta_1) \end{pmatrix} = 0 \quad . \quad (2.30)$$

The fact that  $\sigma$  is second order in  $\Delta\alpha$  and  $\Delta\tau$  shows that  $\sigma$  is the coordinate in the direction perpendicular to the caustic surface, and

$$\hat{\sigma} = -\sin(\theta_1)\hat{\rho} - \cos(\theta_1)\hat{z} \quad (2.31)$$

is the unit normal to the surface, pointing inward.  $\theta(\tau_1)$  is the angle between the  $\rho$  axis and the tangent line at  $(\rho_1, z_1)$ . See Fig. 3.

To obtain the density profile of the caustic near the point under consideration, we need  $D_2(\eta, \sigma)$  to order  $\sqrt{\sigma}$ . So we calculate  $\sigma$  to second order in powers of  $\Delta\alpha$  and  $\Delta\tau$ , and  $D_2$  and  $\eta$  to first order. We find

$$\sigma = \frac{1}{2}(\Delta\alpha \quad \Delta\tau) \begin{pmatrix} s \sin(\theta_1) & -b \cos(\theta_1) \\ -b \cos(\theta_1) & -u \sin(\theta_1) \end{pmatrix} \begin{pmatrix} \Delta\alpha \\ \Delta\tau \end{pmatrix} \quad , \quad (2.32)$$

and

$$\begin{aligned} D_2 &= -b[2s\alpha_1\Delta\alpha + u(2\tau_1 - \tau_0)\Delta\tau] \\ \eta &= [u(\tau_1 - \tau_0)\cos\theta_1 - b\alpha_1\sin\theta_1]\Delta\tau - [s\alpha_1\cos\theta_1 + b\tau_1\sin\theta_1]\Delta\alpha \quad . \end{aligned} \quad (2.33)$$

Eqs. (2.33) can be inverted to obtain  $\Delta\alpha$  and  $\Delta\tau$  as functions of  $D_2$  and  $\eta$ . When the result is inserted into Eq. (2.32), we obtain

$$\sigma(D_2, \eta) = \frac{b}{2\sqrt{(b\tau_1)^2 + (s\alpha_1)^2}} \frac{1}{u\tau_1|3\tau_0 - 4\tau_1|} \left( \tau_1 \left( \frac{D_2}{b} \right)^2 - \frac{us\tau_0\tau_1^2\eta^2}{(b\tau_1)^2 + (s\alpha_1)^2} \right) \quad . \quad (2.34)$$

This implies

$$D_2(\eta, \sigma) = \sqrt{\frac{b^2}{1 + \left(\frac{b^2}{us} - 1\right)\frac{\tau_1}{\tau_0}}\eta^2 + 2b^2u|3\tau_0 - 4\tau_1|\sqrt{\frac{us}{b^2}}(\tau_0 - \tau_1)\tau_1 + \tau_1^2} \sigma \quad . \quad (2.35)$$

Along the  $\hat{\sigma}$  direction ( $\eta = 0$ ), we have

$$D_2(\sigma) = 2C(\tau_1) b\sqrt{\sigma p} \quad , \quad (2.36)$$

with

$$C(\tau_1) = \sqrt{\left|3 - 4\frac{\tau_1}{\tau_0}\right| \sqrt{\frac{us}{b^2} \left(1 - \frac{\tau_1}{\tau_0}\right) \frac{\tau_1}{\tau_0} + \left(\frac{\tau_1}{\tau_0}\right)^2}} . \quad (2.37)$$

Combining Eqs. (2.11) and (2.36), and minding the factor of two because two flows contribute, we have

$$d(\tau_1, \sigma) = \frac{A(\tau_1)}{\sqrt{\sigma}} \Theta(\sigma) \quad (2.38)$$

with

$$A(\tau_1) = \frac{d^2 M}{d\Omega dt} \frac{1}{bC(\tau_1)\sqrt{p}} \frac{\cos(\alpha_1)}{\rho(\tau_1)} . \quad (2.39)$$

In terms of  $A_{0,n} = A_n(\tau_1 = \tau_0)$ , for which estimates are provided in Eq. (2.23), we have

$$A_n(\tau_1) = A_{0,n} \frac{a_n}{\rho_n(\tau_1)} \frac{\cos \alpha_1(\tau_1)}{C_n(\tau_1)} . \quad (2.40)$$

Note that  $A(\tau_1)$  diverges at each of the three cusps because  $C$  vanishes there. In ref. [4] the caustic ring parameters ( $a$ ,  $\tau$ ,  $b$ ,  $u$ ,  $s$ ) are related to the velocity distribution of the flow at last turnaround.

### 3. Curvature radii everywhere

The lensing by a caustic surface depends upon the curvature radius  $R$  of the surface along the line of sight.  $R$  is given by:

$$\frac{1}{R} = \frac{(\cos \omega)^2}{R_1} + \frac{(\sin \omega)^2}{R_2} \quad (2.41)$$

where  $R_1$  and  $R_2$  are the principal curvature radii of the surface and  $\omega$  is the angle between the line of sight and the direction associated with  $R_1$ . In this subsection, we adopt the convention that  $R$  is positive (negative) if, along the line of sight, the surface curves towards (away from) the side with two extra flows. If  $R$  is positive, the surface is called ‘concave’; see Fig. 4. If  $R$  is negative, the surface is called ‘convex’; see Fig. 6. It is a straightforward exercise to calculate the curvature radii of the caustic ring surface at an arbitrary point  $(\alpha_1(\tau_1), \tau_1)$ . We find

$$R_1(\tau_1) = -2 \frac{\sqrt{su}}{b} p \sqrt{\frac{\tau_1}{\tau_0}} \left|3 - 4\frac{\tau_1}{\tau_0}\right| \left(1 - \left(1 - \frac{b^2}{su}\right) \frac{\tau_1}{\tau_0}\right)^{\frac{3}{2}} \quad (2.42)$$

in the direction of the cross-sectional plane of the caustic ring, and

$$R_2(\tau_1) = \pm \frac{\rho_1(\tau_1)}{\sin \theta(\tau_1)} = \pm \frac{\sqrt{su}}{b} \sqrt{\frac{\tau_0}{\tau_1} - 1 + \frac{b^2}{su}} \left(a + \frac{u}{2}(\tau_0 - \tau_1)(\tau_0 - 2\tau_1)\right) , \quad (2.43)$$

in the direction perpendicular to the cross-sectional plane. In Eq. (2.43), the + sign pertains if  $0 \leq \frac{\tau_1}{\tau_0} \leq \frac{3}{4}$ , whereas the - sign pertains if  $\frac{3}{4} \leq \frac{\tau_1}{\tau_0} \leq 1$ .  $R_1$  is always negative except at the three cusps where it vanishes.  $R_2$  diverges at the cusp in the  $z = 0$  plane.

For  $0 \leq \frac{\tau_1}{\tau_0} \leq \frac{3}{4}$ , there is a pair of lines of sight for which the curvature vanishes. They are at angles:

$$\omega = \pm \arctan \sqrt{-\frac{R_2}{R_1}} \quad (2.44)$$

relative to the cross-sectional plane. Gravitational lensing by a fold of zero curvature is discussed in section IV.C.

#### 4. Density near a cusp

In this subsection, we derive the dark matter density profile near a cusp. For the sake of convenience, we choose the cusp in the  $z = 0$  plane at  $\rho = a + p \equiv \rho_0$ , where  $\alpha = \tau = 0$ . Very close to the cusp, we may neglect the term of order  $\tau^2$  in Eqs. (2.10). Hence

$$z = b\alpha\tau, \quad \rho = \rho_0 - u\tau_0\tau - \frac{s}{2}\alpha^2. \quad (2.45)$$

The term of order  $\alpha^2$  cannot be neglected. We define new dimensionless quantities [4]:

$$A \equiv \frac{\alpha}{\tau_0} \sqrt{\frac{s}{u}}, \quad T \equiv \frac{\tau}{\tau_0}, \quad X \equiv \frac{\rho - \rho_0}{p}, \quad Z \equiv \frac{z\sqrt{\zeta}}{p}, \quad (2.46)$$

where  $\zeta = \frac{su}{b^2}$ . In terms of these, Eqs. (2.45) become

$$Z = 2AT, \quad (2.47)$$

$$X = -2T - A^2. \quad (2.48)$$

The Jacobian, Eq. (2.13), becomes:

$$D_2(A, T) = 2bp(T - A^2). \quad (2.49)$$

Substitution of Eq. (2.47) into Eq. (2.48) yields the third order polynomial equation:

$$A^3 + XA + Z = 0. \quad (2.50)$$

The discriminant is:

$$\delta = \left(\frac{Z}{2}\right)^2 + \left(\frac{X}{3}\right)^3. \quad (2.51)$$

If  $\delta > 0$ , the cubic equation has one real root, and two complex roots which are complex conjugate of each other. If  $\delta < 0$ , all the roots are real and unequal. For  $\delta = 0$ , all the roots are real and at least two are equal. The number of real roots is the number of flows at a given location. The tricusp has two flows outside and four inside. However, in the neighborhood of a cusp, one of the flows of the tricusp is non-singular. It does not participate in the cusp

caustic. To include the root corresponding to the non-singular flow near  $(z, \rho) = (0, \rho_0)$ , one must keep the term of order  $\tau^2$  in Eq. (2.45).

$\delta = 0$  is the equation for the caustic surface in physical space. Indeed, Eq. (2.49) implies that at the caustic  $T = A^2$ . Therefore,  $Z = 2T^{3/2}$  and  $X = -3T$ . A straightforward calculation shows that

$$\delta = \frac{D_2}{54bp}(A^4 + 7A^2T - 8T^2). \quad (2.52)$$

Thus  $D_2 = 0$  implies  $\delta = 0$ . However, the converse is not true:  $\delta = 0$  does not imply  $D_2 = 0$  because not all flows at the location of the caustic surface are singular.

Eq. (2.11) for the density becomes

$$d = \frac{1}{2\rho_0bp} \frac{d^2M}{d\Omega dt} \sum_{j=1}^n \frac{1}{|T - A^2|_j}, \quad (2.53)$$

where the sum is over the flows, i.e. the real roots of the cubic polynomial (2.50). If  $\delta > 0$ , the one real root is:

$$A = \left(-\frac{Z}{2} + \sqrt{\delta}\right)^{1/3} + \left(-\frac{Z}{2} - \sqrt{\delta}\right)^{1/3}. \quad (2.54)$$

It describes the one flow outside the cusp. Using Eqs. (2.48, 2.54) in Eq. (2.53) we obtain

$$d = \frac{1}{\rho_0bp} \frac{d^2M}{d\Omega dt} \frac{1}{|X - 3\left(-\frac{Z}{2} + \sqrt{\delta}\right)^{2/3} - 3\left(\frac{Z}{2} + \sqrt{\delta}\right)^{2/3}|}. \quad (2.55)$$

Just above or below the cusp, where  $X = 0$  and  $|Z| \ll 1$ , we have

$$d = \frac{1}{3bp\rho_0} \frac{d^2M}{d\Omega dt} \frac{1}{|Z|^{2/3}}. \quad (2.56)$$

On the other hand, if we approach the cusp in the plane of the ring from the outside, where  $Z = 0$  and  $0 < X \ll 1$ , we find

$$d = \frac{1}{b\rho_0} \frac{d^2M}{d\Omega dt} \frac{1}{(\rho - \rho_0)}. \quad (2.57)$$

Next, we calculate the density inside the cusp, where  $\delta < 0$ . The three real roots of the polynomial (2.50) are:

$$A_1 = 2\sqrt{\frac{-X}{3}} \cos \theta \quad (2.58)$$

$$A_2 = 2\sqrt{\frac{-X}{3}} \cos \left(\theta + \frac{2\pi}{3}\right) \quad (2.59)$$

$$A_3 = 2\sqrt{\frac{-X}{3}} \cos \left(\theta + \frac{4\pi}{3}\right), \quad (2.60)$$

where  $\cos 3\theta \equiv -\frac{Z}{2} \left(-\frac{3}{X}\right)^{3/2}$  and  $0 \leq \theta \leq \frac{\pi}{3}$ . Inserting them into Eq. (2.53) and using Eq. (2.48), we obtain

$$d = \frac{1}{b p \rho_0} \frac{d^2 M}{d\Omega dt} \left( \frac{1}{-X} \right) \left( \frac{1}{4 \cos^2(\theta) - 1} + \frac{1}{4 \cos^2(\theta + \frac{2\pi}{3}) - 1} + \frac{1}{1 - 4 \cos^2(\theta + \frac{4\pi}{3})} \right) , \quad (2.61)$$

where each term in the parentheses corresponds to one of the three flows. Adding the individual flow densities yields:

$$d = \frac{2}{b p \rho_0} \frac{d^2 M}{d\Omega dt} \frac{1}{|X|} \frac{1}{(\sqrt{3} - \tan \theta) \sin 2\theta} . \quad (2.62)$$

If we approach the cusp in the galactic plane from the inside, where  $Z = 0$  and  $0 < -X \ll 1$ , we have

$$d = \frac{2}{b \rho_0} \frac{d^2 M}{d\Omega dt} \frac{1}{(\rho_0 - \rho)} , \quad (2.63)$$

which is twice the result in Eq. (2.57). The gravitational lensing properties of a cusp are derived, for a special line of sight, in subsection IV.D.

### III. GENERAL FORMALISM

The first part of this section gives a brief account of the gravitational lensing formalism [14]. In the second part we show how this formalism can be streamlined in the special case of lensing by dark matter caustics.

In linear approximation, the deflection angle  $\vec{\theta}$  of a light ray due to a gravitational field is given by:

$$\vec{\theta} = \vec{\nabla} \frac{2}{c^2} \int \Phi dy \quad (3.1)$$

where  $\Phi$  is the Newtonian potential. We choose the  $y$ -axis in the direction of propagation of light. The deflection angle  $\vec{\theta}$  is related to the angular shift  $\vec{\xi}_I - \vec{\xi}_S$  on the sky of the apparent direction of a source:

$$\vec{\theta}(\vec{\xi}_I) = \frac{D_S}{D_{LS}} (\vec{\xi}_I - \vec{\xi}_S) \quad (3.2)$$

where  $D_S$  and  $D_{LS}$  are the distances of the source to the observer and to the lens respectively.  $\vec{\xi}_S$  is the angular position of the source in the absence of the lens whereas  $\vec{\xi}_I$  is the angular position of the image with the lens present. The angles carry components in the  $x$  and  $z$ -directions:  $\vec{\theta} = (\theta_x, \theta_z)$ ,  $\vec{\xi} = (\xi_x, \xi_z)$ , etc. Unless otherwise stated, we mean by a vector a quantity with components in the  $x$ - and  $z$ -directions.

It is convenient to introduce a 2-D potential

$$\psi(\vec{\xi}_I) = \frac{2D_{LS}}{c^2 D_L D_S} \int dy \Phi , \quad (3.3)$$

so that

$$\vec{\theta} = \frac{D_S}{D_{LS}} \vec{\nabla}_{\xi_I} \psi(\vec{\xi}_I) \quad , \quad (3.4)$$

where  $\vec{\nabla}_{\xi_I} = D_L \vec{\nabla}$ .  $D_L$  is the distance of the observer to the lens. Eq. (3.2) then becomes:

$$\vec{\xi}_I = \vec{\xi}_S + \vec{\nabla}_{\xi_I} \psi(\vec{\xi}_I) \quad . \quad (3.5)$$

It gives the map  $\vec{\xi}_S(\vec{\xi}_I)$  from the image plane to the source plane. The inverse map may be one to one, or one to many. In the latter case, there are multiple images and infinite magnification when a pair of images merges.

Our problem is to find the image map of a point source when the matter distribution is given. The 2-D gravitational potential  $\psi$  obeys the Poisson equation:

$$\nabla_{\xi_I}^2 \psi = \frac{8\pi G}{c^2} \frac{D_L D_{LS}}{D_S} \Sigma = 2 \frac{\Sigma}{\Sigma_c} \quad , \quad (3.6)$$

where  $\Sigma(\xi_{Ix}, \xi_{Iz})$  is the column density, i.e. the integral of the volume density along the line of sight:

$$\Sigma(\vec{\xi}_I) = \int dy d(D_L \xi_{Ix}, y, D_L \xi_{Iz}) \quad , \quad (3.7)$$

and  $\Sigma_c$  is the critical surface density:

$$\Sigma_c = \frac{c^2 D_S}{4\pi G D_L D_{LS}} = 0.347 \text{ g/cm}^2 \left( \frac{D_S}{D_L D_{LS}} \text{ Gpc} \right) . \quad (3.8)$$

It is such that a uniform sheet of density  $\Sigma_c$  focuses radiation from the source to the observer.

Eq. (3.6) is solved by:

$$\psi(\vec{\xi}_I) = \frac{1}{\pi \Sigma_c} \int d^2 \xi'_I \Sigma(\vec{\xi}'_I) \ln |\vec{\xi}_I - \vec{\xi}'_I| \quad , \quad (3.9)$$

and hence

$$\Delta \vec{\xi} \equiv \vec{\xi}_I - \vec{\xi}_S = \vec{\nabla}_{\xi_I} \psi(\vec{\xi}_I) = \frac{1}{\pi \Sigma_c} \int d^2 \xi'_I \Sigma(\vec{\xi}'_I) \frac{\vec{\xi}_I - \vec{\xi}'_I}{(\vec{\xi}_I - \vec{\xi}'_I)^2} \quad . \quad (3.10)$$

The image structure, distortion and magnification are given by the Jacobian matrix of the map  $\vec{\xi}_S(\vec{\xi}_I)$  from image to source:

$$K_{ij} \equiv \frac{\partial \xi_{Si}}{\partial \xi_{Ij}} = \delta_{ij} - \psi_{ij} \quad (3.11)$$

where  $\psi_{ij} \equiv \frac{\partial^2 \psi}{\partial \xi_{Ii} \partial \xi_{Ij}}$ . Because gravitational lensing does not change surface brightness, the magnification  $\mathcal{M}$  is the ratio of image area to source area. Therefore

$$\mathcal{M} = \frac{1}{|\det(K_{ij})|} \quad . \quad (3.12)$$



To first order, for  $\psi_{ij} \ll 1$ ,

$$\mathcal{M} = 1 + \nabla_{\xi_I}^2 \psi = 1 + 2 \frac{\Sigma}{\Sigma_c} \quad . \quad (3.13)$$

To get the largest lensing effects, we wish to minimize  $\Sigma_c$ , given in Eq. (3.8). For fixed  $D_S$ , the minimum occurs when the lens is situated half way between the source and the observer. Also  $D_S$  should be as large as possible. For our estimates, we will assume that the source is at cosmological distances, e.g.  $2D_L = 2D_{LS} = D_S = 1\text{Gpc}$ , in which case  $\Sigma_c = 1.39 \text{ g/cm}^2$ .

For a general mass distribution, the gravitational lensing effects are obtained by first calculating the column density, Eq. (3.7), and then the image shift, Eq. (3.10). This procedure can be simplified when the lens is a dark matter caustic. We are interested in lines of sight which are tangent to a caustic surface, because the column density  $\Sigma$  has the highest contrast there. We assume that, in the neighborhood of the tangent point, the flow is independent of  $y$  except for a shift  $\vec{x}(y)$  of the caustic surface with  $y$ . The density can then be written as:

$$d(x, y, z) = d(x - x(y), z - z(y)) \quad , \quad (3.14)$$

where  $d(x, z)$  is the density of the 2-D flow in the plane orthogonal to the line of sight. The flow in the  $y$ -direction is irrelevant because lensing depends only on the column density  $\Sigma$ .

In the limit of zero velocity dispersion, a 2-D flow is specified by giving the spatial coordinates  $\vec{x}(\alpha, \beta, t)$  of the particle labeled  $(\alpha, \beta)$  at time  $t$ , for all  $(\alpha, \beta, t)$ . The labels  $\alpha$  and  $\beta$  are chosen arbitrarily. At a given time  $t$ ,  $\vec{x}(\alpha, \beta, t) = \vec{x}$  has a discrete number of solutions  $(\alpha, \beta)_j(\vec{x}, t)$  labeled by  $j = 1, \dots, n(\vec{x}, t)$ .  $n$  is the number of distinct flows at  $(\vec{x}, t)$ . Here,  $t$  is the time at which the light ray passes by the caustic. Henceforth we will not show the time dependence explicitly. The particle density in physical space is:

$$d(x, z) = \sum_{j=1}^{n(\vec{x})} \frac{d^2 \Lambda}{d\alpha d\beta} \frac{1}{\left| \frac{\partial(x, z)}{\partial(\alpha, \beta)} \right|} \Big|_{(\alpha, \beta) = (\alpha, \beta)_j(\vec{x})} \quad . \quad (3.15)$$

where  $\Lambda$  is the mass per unit length in the direction of the line of sight and  $\frac{d^2 \Lambda}{d\alpha d\beta}$  is the  $\Lambda$  density in parameter space. Inserting Eqs. (3.7) and (3.14) into Eq. (3.10) we obtain:

$$\vec{\nabla}_{\xi_I} \psi(\vec{\xi}_I = \vec{x}/D_L) = \frac{1}{\pi \Sigma_c} \int dy \int d^2 \xi'_I \frac{\vec{\xi}_I - \vec{\xi}'_I}{|\vec{\xi}_I - \vec{\xi}'_I|^2} d(D_L \xi'_{Ix} - x(y), D_L \xi'_{Iz} - z(y)) \quad . \quad (3.16)$$

When  $d$  is replaced by the caustic density (3.15), Eq.(3.16) becomes:

$$\vec{\nabla}_{\xi_I} \psi(\vec{\xi}_I = \vec{x}/D_L) = \frac{1}{\pi \Sigma_c D_L} \int dy \int dx' dz' \frac{\vec{x} - \vec{x}'}{(\vec{x} - \vec{x}')^2} \sum_{j=1}^n \frac{1}{\left| \frac{\partial(x', z')}{\partial(\alpha, \beta)} \right|} \frac{d^2 \Lambda}{d\alpha d\beta} \Big|_{(\alpha, \beta) = (\alpha, \beta)_j(\vec{x}' - \vec{x}(y))} \quad . \quad (3.17)$$

Changing variables from  $(x', z')$  to  $(\alpha, \beta)$  and assuming that the density in parameter space varies only slowly over the region of integration, we rewrite Eq. (3.17) as:

$$\vec{\nabla}_{\xi_I} \psi(\vec{\xi}_I = \vec{x}/D_L) = \frac{1}{\pi \Sigma_c D_L} \frac{d^2 \Lambda}{d\alpha d\beta} \int dy \int d\alpha d\beta \frac{\vec{x} - \vec{x}(\alpha, \beta) - \vec{x}(y)}{|\vec{x} - \vec{x}(\alpha, \beta) - \vec{x}(y)|^2} \quad . \quad (3.18)$$

Further simplification is achieved by defining the complex integral:

$$I(x, z) \equiv \int d\alpha d\beta \frac{1}{x - x(\alpha, \beta) + i(z - z(\alpha, \beta))} \quad , \quad (3.19)$$

in terms of which the shifts are given by:

$$\begin{aligned} \Delta\xi_x &= \frac{\partial\psi}{\partial\xi_{Ix}} = \frac{1}{\pi\Sigma_c D_L} \frac{d^2\Lambda}{d\alpha d\beta} \operatorname{Re} \int dy I(\vec{x} - \vec{x}(y)) \quad , \\ \Delta\xi_z &= \frac{\partial\psi}{\partial\xi_{Iz}} = -\frac{1}{\pi\Sigma_c D_L} \frac{d^2\Lambda}{d\alpha d\beta} \operatorname{Im} \int dy I(\vec{x} - \vec{x}(y)) \quad . \end{aligned} \quad (3.20)$$

Eqs. (3.19) and (3.20) are useful when the caustic has contrast in the two dimensions transverse to the line of sight, e.g. near a cusp.

However, in many applications, the caustic has contrast in only one of the dimensions transverse to the line of sight. Choosing  $\hat{x}$  to be the trivial direction, Eq. (3.6) is reduced to:

$$\frac{d^2\psi}{d\xi_I^2}(\xi_I) = \frac{2}{\Sigma_c} \Sigma(z = D_L \xi_I) \quad , \quad (3.21)$$

and the column density is given by:

$$\Sigma(\xi_I) = \int dy d(z - z(y)) \quad . \quad (3.22)$$

The flow is now effectively one dimensional. Its physical space density is given by

$$d(z) = \sum_{j=1}^{n(z)} \frac{d\Lambda}{d\alpha} \frac{1}{\left| \frac{dz}{d\alpha} \right|} \Big|_{\alpha=\alpha_j(z)} \quad , \quad (3.23)$$

where  $\Lambda$  is the mass surface density in the two trivial directions ( $x$  and  $y$ ) and  $\frac{d\Lambda}{d\alpha}$  is the  $\Lambda$  density in parameter space. The 1-D Green's function is  $G = \frac{1}{2}(|\xi| + a\xi) + b$ , where  $a$  and  $b$  are arbitrary constants. The shift is:

$$\frac{d\psi}{d\xi_I}(\xi_I) = \frac{1}{\Sigma_c} \int d\xi'_I \Sigma(\xi'_I) (\operatorname{Sign}(\xi_I - \xi'_I) + a) \quad . \quad (3.24)$$

The constant  $a$  causes an overall shift of the image, which does not concern us. We choose  $a = -1$ . Repeating the steps done earlier for the 2-D case, Eq. (3.24) is re-expressed as:

$$\Delta\xi = -\frac{2}{\Sigma_c D_L} \frac{d\Lambda}{d\alpha} \int dy \int d\alpha \Theta(-z + z(\alpha) + z(y)) \quad . \quad (3.25)$$

In the next section Eq. (3.25) is used to calculate the shifts due to simple folds of dark matter flows, and Eq. (3.20) for the shifts due to a cusp.

## IV. APPLICATIONS

### A. Lensing by a concave fold

We consider a simple fold caustic which has curvature radius  $R$  along the line of sight. We assume that the surface is concave, i.e. it is curved in the direction of the two extra flows. See Fig. 4. The outer caustics of dark matter halos are examples of concave caustic surfaces. The convex case is discussed in the next subsection.

In the neighborhood of the point  $P$  of closest approach of the line of sight with the caustic surface, we choose coordinates such that  $\hat{z}$  is perpendicular to the surface whereas  $\hat{x}$  and the direction  $\hat{y}$  of the line of sight are parallel.  $P$  has coordinates  $x = y = z = 0$ . In the  $y = 0$  plane, the flow is given by  $z(\alpha) = -\frac{1}{2}h\alpha^2$ , where  $h$  is a positive constant. Using Eq. (3.23) we find the density in the  $y = 0$  plane:

$$d(\sigma) = A \frac{\Theta(\sigma)}{\sqrt{\sigma}} \quad , \quad (4.1)$$

where  $\sigma = -z$ , and

$$A = \sqrt{\frac{2}{h}} \frac{d\Lambda}{d\alpha} \quad . \quad (4.2)$$

For  $y \neq 0$ , the density is still given by Eq. (4.1) but with  $\sigma = z(y) - z$  and  $z(y) = -\frac{y^2}{2R}$ . We calculate the shift using Eq. (3.25):

$$\begin{aligned} \Delta\xi &= -\frac{2}{\Sigma_c D_L} \frac{d\Lambda}{d\alpha} \int_{-\sqrt{-2Rz}}^{\sqrt{-2Rz}} dy \int d\alpha \Theta\left(-z - \frac{h}{2}\alpha^2 - \frac{y^2}{2R}\right) \\ &= \frac{4\pi}{\Sigma_c} \frac{d\Lambda}{d\alpha} \sqrt{\frac{R}{h}} \Theta(-\xi_I) \xi_I \quad . \end{aligned} \quad (4.3)$$

Hence

$$\Delta\xi = \xi_I - \xi_S = \eta \xi_I \Theta(-\xi_I) \quad , \quad (4.4)$$

with

$$\eta = \frac{2\pi A \sqrt{2R}}{\Sigma_c} \quad . \quad (4.5)$$

One can also obtain this result by calculating the column density:

$$\Sigma(\xi_I) = \int dy d(y, z = \xi_I) = \int dy \frac{A \Theta(-\xi_I D_L - \frac{y^2}{2R})}{\sqrt{-\xi_I D_L - \frac{y^2}{2R}}} = \pi A \sqrt{2R} \Theta(-\xi_I) \quad , \quad (4.6)$$

and solving Eq. (3.6):

$$\xi_I - \xi_S = \frac{d\psi}{d\xi_I} = \frac{2}{\Sigma_c} \int d\xi_I \Sigma(\xi_I) = \eta \xi_I \Theta(-\xi_I) \quad . \quad (4.7)$$

Eqs. (4.6, 4.7) were first obtained by Hogan [6]. The agreement with Eq. (4.4) validates the formalism derived in section III. Fig. 5 plots the source position  $\xi_S$  versus the image position  $\xi_I$ .

The magnification is:

$$\mathcal{M} = \frac{d\xi_I}{d\xi_S} = 1 + \eta \Theta(-\xi_I) + 0(\eta^2) \quad . \quad (4.8)$$

When the line of sight of a moving source crosses the surface of a simple concave fold, the component of its apparent velocity perpendicular to the fold changes abruptly. Also, a discontinuity occurs in the magnification of the image. Both effects are of order  $\eta$ .

We estimate  $\eta$  for the outer caustics of galactic halos using Eqs. (2.5 - 2.8):

$$\left\{ \eta_n = \frac{\sqrt{2} v_{\text{rot}}^2}{G \Sigma_c} \frac{F_n}{R_n} : n = 1, 2, \dots \right\} \sim (7, 6, 6, 6, 6, \dots) \cdot 10^{-3} \cdot \left( \frac{D_L D_{LS}}{D_S \text{ Gpc}} \right) \left( \frac{v_{\text{rot}}}{220 \text{ km/s}} \right) \left( \frac{h}{0.7} \right) \quad . \quad (4.9)$$

A magnification of order  $10^{-2}$  seems hard to observe. However, the images of extended sources may be modified in recognizable ways. In particular, straight jets would be seen with an abrupt bend where their line of sight crosses a fold. Indeed the image is stretched by the factor  $1 + \eta$  in the direction perpendicular to the caustic, on the side with the two extra flows. If the jet makes angle  $\alpha$  with the normal, it appears bent by an angle  $\delta \equiv \frac{1}{2} \eta \sin(2\alpha)$ . Searching the sky for bends in extended sources may be a realistic approach to detecting caustic structure in galactic halos [6].

## B. Lensing by a convex fold

By definition, a convex fold is curved in the direction opposite to the side with two extra flows. See Fig. 6. Using the conventions of the previous subsection, we write the equation for the displacement of the surface along the line of sight as  $z(y) = \frac{y^2}{2R}$ , and that for the flow as  $z(\alpha) = -\frac{1}{2} h \alpha^2$ , for small  $z$ , with  $R, h > 0$ . Eqs. (4.1) and (4.2) still apply, with  $\sigma = y^2/2R - z$ . Eq. (3.25) yields the shift:

$$\Delta\xi = -\frac{8}{\Sigma_c D_L} \frac{d\Lambda}{d\alpha} \left\{ \Theta(-\xi_I) \int_0^\infty dy + \Theta(\xi_I) \int_{\sqrt{2RD_L\xi_I}}^\infty dy \right\} \sqrt{\frac{2}{h} \left( \frac{y^2}{2R} - D_L \xi_I \right)} \quad . \quad (4.10)$$

We introduce a cut-off  $L$  for the integral over large  $y$ .  $L$  can be thought of as the length scale beyond which our description of the flow is invalid. The above equation becomes:

$$\Delta\xi = -\frac{4}{\Sigma_c D_L} \frac{d\Lambda}{d\alpha} \frac{1}{\sqrt{hR}} \left\{ L \sqrt{L^2 - 2RD_L\xi_I} - 2RD_L\xi_I \ln \left( \frac{L + \sqrt{L^2 - 2RD_L\xi_I}}{\sqrt{2RD_L|\xi_I|}} \right) \right\} \quad . \quad (4.11)$$

By expanding Eq. (4.11) in powers of  $\frac{1}{L}$ , and using Eq. (4.2), we obtain the  $\xi_I$ -dependent shift:

$$\Delta\xi = \xi_I - \xi_S = -\frac{\eta'}{\pi} \left[ \ln \left( \frac{RD_L |\xi_I|}{2L^2} \right) - 1 \right] \xi_I \quad , \quad (4.12)$$

where  $\eta'$  is [like  $\eta$  in Eq. (4.5)] given by

$$\eta' = \frac{2\pi A\sqrt{2R}}{\Sigma_c} \quad . \quad (4.13)$$

The magnification is :

$$\mathcal{M} = \frac{d\xi_I}{d\xi_S} = \left| 1 + \frac{\eta'}{\pi} \ln \left( \frac{RD_L |\xi_I|}{2L^2} \right) \right|^{-1} \quad . \quad (4.14)$$

The cut-off  $L$  has an effect on both the magnification and the elongation of the image in the direction normal to the caustic surface, but that effect is  $\xi_I$  independent.  $L$  has a global effect on the image, as opposed to an effect localized near  $\xi_I = 0$ .

Fig. 7 plots  $\xi_S$  versus  $\xi_I$ . It shows that a convex fold can cause a triple image of a point source. In particular, when the source is exactly behind the caustic ( $\xi_S = 0$ ), the images are at  $\xi_I = -\xi_c, 0$ , and  $+\xi_c$ , with

$$\xi_c = \frac{2L^2}{RD_L} \exp \left( -\frac{\pi}{\eta'} + 1 \right) \quad . \quad (4.15)$$

Sufficiently far from the caustic, a point source has a single image, say at  $\xi_{I1} > 0$ . When the line of sight approaches the caustic surface tangent point, two new images appear on top of each other at  $\xi_{I2} = \xi_{I3} = -\xi_c/e$ . At that moment, the magnification at  $\xi_{I2}$  is infinite, and  $\xi_S = \eta'\xi_c/e\pi$ . As the source crosses the caustic,  $\xi_{I2}$  moves towards  $\xi_{I1}$  and finally merges with it. When  $\xi_{I1} = \xi_{I2} = +\xi_c/e$ , the magnification diverges again. After that, only the image at  $\xi_{I3}$  remains.

Let us apply the above results to the line of sight in the plane of a caustic ring at the sample point, ( $z = 0, \rho = a$ ), discussed in subsection II.B.1. Setting  $R = a_n$  and using Eq. (2.22) we obtain for the  $n$ th ring

$$\eta'_n = \frac{2\pi A_{0,n}\sqrt{2a_n}}{\Sigma_c} = \frac{v_{\text{rot}}^2}{\sqrt{2G}\Sigma_c} \frac{f_n}{\sqrt{a_n p_n}} \frac{v_n}{b_n} \quad . \quad (4.16)$$

Using Eq. (2.23) to estimate  $A_{0,n}$ , we find

$$\begin{aligned} \{\eta'_n : n = 1, 2, \dots\} &\sim (5, 4, 4, 4, 4, \dots) \cdot 10^{-2} \frac{D_L D_{LS}}{D_S \text{ Gpc}} \\ &\cdot \left( \frac{0.27}{j_{\text{max}}} \right) \left( \frac{h}{0.7} \right) \left( \frac{v_{\text{rot}}}{220 \text{ km/s}} \right) \quad . \end{aligned} \quad (4.17)$$

For such small values of  $\eta'$  the angular distance between the triple images is exponentially small and unresolvable with present and foreseeable instruments.

The image of an extended object is stretched in the direction perpendicular to the caustic by the relative amount

$$\mathcal{M} - 1 = -\frac{\eta'}{\pi} \ln \left( \frac{RD_L |\xi_I|}{2L^2} \right) . \quad (4.18)$$

The image is stretched for  $\xi_I < \xi_d$ , and compressed for  $\xi_I > \xi_d$ , where

$$\xi_d = \frac{2L^2}{RD_L} . \quad (4.19)$$

In the case of the sample point ( $z = 0, \rho = a$ ) with line of sight in the  $z = 0$  plane, the cut-off length  $L$ , i.e. the distance in the  $y$ -direction over which our description of the flow is valid, is of order  $\sqrt{2ap}$ . In that case  $\xi_d \sim 4p/D_L$ . Since  $p/D_L$  is the transverse angular size of the caustic ring, our description certainly fails for  $\xi_I > p/D_L$ . So, over the region where our calculation is valid, the image is magnified. The effects are generically of order one percent, increasing to several percent when  $\xi_I \sim 10^{-3}\xi_d$ , for caustic rings at cosmological distances.

### C. Lensing by a fold with zero curvature

We saw in section II.B.3 that the surface of a caustic ring has tangent lines along which the curvature vanishes. One may speculate that the lensing effects of a caustic surface are strongest when the line of sight is tangent to the surface in a direction of zero curvature, because the line of sight stays close to the caustic over greater depths in that case. If the line of sight of an observer looking at the outside profile of a caustic ring is, at some point on the profile, in a direction of zero curvature, then the equation for the intersection of the caustic surface with the plane containing the outward normal to the surface ( $\hat{z}$ ) and the line of sight ( $\hat{y}$ ) is  $z(y) = -\frac{y^4}{4U}$  where  $U$  is positive and has dimensions of (length)<sup>3</sup>. In such a case, the cubic term in the Taylor expansion of  $z(y)$  is absent because the line of sight remains everywhere outside the caustic ring tube. We did not calculate  $U$  for caustic rings but expect  $U \sim (\text{kpc})^3$  in order of magnitude. The flow is given by  $z(\alpha) = -\frac{1}{2}h\alpha^2$  with  $h > 0$ , as before, and Eq. (4.2) holds.

Using the above expressions for  $z(y)$  and  $z(\alpha)$  in Eq. (3.25), we find the shift

$$\begin{aligned} \Delta\xi &= -\frac{2}{\Sigma_c D_L} \frac{d\Lambda}{d\alpha} \int dy \int d\alpha \Theta \left( -z - \frac{1}{2}h\alpha^2 - \frac{y^4}{4U} \right) \\ &= -\frac{8}{\Sigma_c D_L} \frac{d\Lambda}{d\alpha} \frac{(-4Uz)^{3/4}}{\sqrt{2hU}} \Theta(-\xi_I) \int_0^1 dt \sqrt{1-t^4} \\ &= -\Theta(-\xi_I) \left( -\xi_0 \xi_I^3 \right)^{1/4} , \end{aligned} \quad (4.20)$$

where

$$\xi_0 = \left( 9.89 \frac{A}{\Sigma_c} \right)^4 \frac{U}{D_L} . \quad (4.21)$$

The magnification is:

$$\mathcal{M} = \left| 1 - \frac{3}{4} \Theta(-\xi_I) \left( -\frac{\xi_0}{\xi_I} \right)^{1/4} \right|^{-1} . \quad (4.22)$$

Fig. 8 shows  $\xi_S$  versus  $\xi_I$ . Triple images occur when  $|\xi_I| \lesssim \xi_0$ . Unfortunately, for the zero curvature tangents of caustic rings envisaged above,  $\xi_0$  is very small. For  $2D_L = 2D_{LS} = D_S = \text{Gpc}$ ,  $A = 3 \cdot 10^{-4} \frac{\text{gr}}{\text{cm}^2 \text{kpc}^{\frac{1}{2}}}$ , and  $U = (\text{kpc})^3$ , one finds  $\xi_0 = 4 \cdot 10^{-17}$ . Hence the triple images cannot be resolved. Also, even at angular distances as small as  $\xi_I \sim 10^{-9}$ , the magnification and image distortion is only of order 1%.

#### D. Lensing by a cusp

In this subsection, we investigate a line of sight parallel to the plane ( $z = 0$ ) of a caustic ring, and passing near the cusp at  $\rho = \rho_0$ . See Fig. 9. We use the 2-D lensing equations derived in section III. The shifts are given by Eq. (3.20) in terms of the complex integral  $I$  of Eq. (3.19). Using Eq. (2.45), we have

$$I = \int d\alpha \int d\tau \frac{1}{\rho - a - \frac{1}{2}u\tau_0^2 + u\tau_0\tau + \frac{1}{2}s\alpha^2 + i(z - b\alpha\tau)} \quad . \quad (4.23)$$

Because we are close to the cusp, the term of order  $\tau^2$  is neglected in the denominator of the integrand. In terms of the parameters defined in Eqs. (2.46),

$$I = \frac{2}{b\sqrt{\zeta}} \int dT \int_{-\infty}^{\infty} \frac{dA}{A^2 - 2i\frac{AT}{\sqrt{\zeta}} + 2T + X + i\frac{Z}{\sqrt{\zeta}}} \quad . \quad (4.24)$$

The integration over  $A$  yields

$$I = \frac{2\pi}{b\sqrt{\zeta}} \int_{\frac{|T|}{\sqrt{\zeta}} < C} \frac{dT}{\sqrt{\frac{T^2}{\zeta} + 2T + X + i\frac{Z}{\sqrt{\zeta}}}} \quad , \quad (4.25)$$

where  $C \equiv \text{Re} \sqrt{\frac{T^2}{\zeta} + 2T + X + i\frac{Z}{\sqrt{\zeta}}} > 0$ . Near the cusp ( $X, Z \ll 1$ ) the terms of order  $T^2$  can be neglected since they are unimportant in the denominator of Eq. (4.24). Eq. (4.25) becomes then:

$$I(X, Z) = \frac{2\pi}{b\sqrt{\zeta}} \int \frac{dT}{\sqrt{2T + X + i\frac{Z}{\sqrt{\zeta}}}} \quad , \quad (4.26)$$

where the integration domain is defined by the inequality:

$$T^4 - \zeta(2T^3 + XT^2) - \frac{\zeta Z^2}{4} < 0 \quad . \quad (4.27)$$

Let us call  $T_i$  ( $i = 1, \dots, 4$ ) the roots of the polynomial on the left hand side of (4.27). Near the cusp, three of the roots  $T_i$  are near zero and one of the roots is close to  $2\zeta$ . Let us call the latter  $T_4$ . In order to find the roots near  $T = 0$  we neglect the quartic term and solve the cubic equation:

$$T^3 + \frac{X}{2}T^2 + \frac{Z^2}{8} = 0 \quad . \quad (4.28)$$

This equation is also obtained by eliminating  $A$  from Eqs. (2.47) and (2.48). Hence the solutions of Eq. (4.28) are the values of  $T$  for the flows near the cusp. As was discussed in section II.B.4, the number of flows is determined by  $\delta$ , given in Eq. (2.51). Outside the cusp, where  $\delta > 0$ , there is a single root  $T_1$ . Inside the cusp where  $\delta < 0$ , there are three roots  $T_1, T_2$  and  $T_3$ . Fig. 10 shows the quartic polynomial, Eq. (4.27), for various values of  $X$  and  $Z$ , and  $\zeta = 1$ .

For a line of sight just outside the cusp, the quartic polynomial is negative from  $T_1$  to  $T_4$  with:

$$T_1 = -\frac{1}{2} \left( \sqrt{\delta} - \frac{|Z|}{2} \right)^{2/3} - \frac{1}{2} \left( \sqrt{\delta} + \frac{|Z|}{2} \right)^{2/3} - \frac{X}{6} \quad . \quad (4.29)$$

Eq. (4.26) becomes in that case:

$$I = \frac{2\pi}{b\sqrt{\zeta}} \left\{ \sqrt{2T_4 + X + i\frac{Z}{\sqrt{\zeta}}} - \sqrt{2T_1 + X + i\frac{Z}{\sqrt{\zeta}}} \right\} \quad . \quad (4.30)$$

Let us consider the line of sight defined by Fig. 9. Eq. (3.20) gives the shift in the direction perpendicular to the plane of the cusp as

$$\Delta\xi_z = -\frac{1}{\pi\Sigma_c D_L} \frac{d^2\Lambda}{d\alpha d\tau} \text{Im} \int dy I(X - X(y), Z) \quad (4.31)$$

where  $X(y) = -\frac{y^2}{2\rho_0 p}$  is the shift of the cusp as a function of depth. The integral in Eq. (4.31) with the integrand given by Eqs. (4.29) and (4.30) can be done numerically. Here we only give a rough estimate, to determine the order of magnitude and qualitative properties of the lensing effects.

For  $X = 0$  and  $Z \ll 1$ , we have

$$I = \frac{2\pi}{b} \left[ 2 - \frac{i}{\sqrt{\zeta}} \text{Sign}(Z) |Z|^{1/3} - \frac{1}{2\zeta} |Z|^{2/3} \right] + O(Z) \quad . \quad (4.32)$$

Because the scaling law  $X^3 \sim Z^2$  holds close to the cusp, we expect Eq. (4.32) to be valid as long as the shift in the  $x$ -direction  $|\Delta X| \lesssim |Z|^{2/3}$ . Hence Eq. (4.32) provides a good estimate of  $I(X - X(y), Z)$  over a depth  $2\Delta y$  with  $\Delta y \sim \sqrt{2\rho_0 p} |Z|^{1/3}$ . Therefore

$$\Delta\xi_z \sim \frac{2}{\Sigma_c D_L b} \sqrt{\frac{2\rho_0 p}{\zeta}} \frac{d^2\Lambda}{d\alpha d\tau} |Z|^{2/3} \text{Sign}(Z) \quad . \quad (4.33)$$

Since we are near  $\alpha = 0$ ,

$$\frac{d^2\Lambda}{d\alpha d\tau} = \frac{1}{2\pi\rho_0} \frac{d^2 M}{d\alpha d\tau} = \frac{1}{\rho_0} \frac{d^2 M}{d\Omega dt} \quad . \quad (4.34)$$

Using this and Eq. (2.18), we obtain

$$\Delta\xi_z \sim \eta'' |\xi_{Iz}|^{2/3} \text{Sign}(\xi_{Iz}) \quad , \quad (4.35)$$



where

$$\eta'' \equiv \frac{2\sqrt{2}a}{\zeta^{\frac{1}{6}}\Sigma_c D_L^{\frac{1}{3}}} p^{\frac{1}{3}} A_0 \quad . \quad (4.36)$$

The contribution to the magnification from distortion in the  $z$ -direction is therefore:

$$\mathcal{M}_z \sim \left| 1 - \eta'' \frac{2}{3} |\xi_{Iz}|^{-\frac{1}{3}} \right|^{-1} \quad . \quad (4.37)$$

Fig. 11 plots  $\xi_{Sz}$  versus  $\xi_{Iz}$ . For  $\xi_{Iz} \lesssim \xi_1 \sim \eta''^3$ , a point source has triple images. For the  $n$ th caustic ring,  $\eta''$  can be estimated using Eqs. (2.19, 2.23), and assuming  $p \simeq 0.1a$ ,  $\zeta \sim 1$ :

$$\begin{aligned} \{\eta''_n : n = 1, 2, \dots\} &\sim (1.5, 1, 0.7, 0.6, 0.5, \dots) \cdot 10^{-4} \frac{D_L^{\frac{2}{3}} D_{LS}}{D_S \text{ Gpc}^{\frac{2}{3}}} \cdot \\ &\cdot \left(\frac{0.27}{j_{\max}}\right)^{\frac{2}{3}} \left(\frac{h}{0.7}\right)^{\frac{2}{3}} \left(\frac{v_{\text{rot}}}{220 \text{ km/s}}\right)^{\frac{4}{3}} \quad . \quad (4.38) \end{aligned}$$

At cosmological distances, the typical angular separation between the images is of order  $10^{-12}$ . Unfortunately, here again, the images are too close to be resolved. However, for an angular distance  $\xi_I \sim 10^{-9}$ ,  $\mathcal{M}_z$  is of order 10%, which may be observable. The lensing properties of a cusp for other lines of sight can be calculated numerically using Eqs. (3.20) and (4.23). The latter equation is replaced by Eqs. (4.30) and (4.29), and  $T_4 = 2\zeta$ , if the line of sight is everywhere outside the region with two extra flows.

## V. CONCLUSIONS

The dark matter caustics present in the halos of isolated galaxies were discussed in Section II. They are of two types, outer and inner. The outer caustics are topological spheres surrounding the galaxy and labeled by  $n = 1, 2, 3, \dots$ . Each is a simple fold ( $A_2$ ) catastrophe located near where a dark matter outflow reaches its furthest distance from the galactic center before falling back in. The inner caustics are rings in or near the galactic plane. They are also labeled by  $n = 1, 2, 3, \dots$ . A caustic ring is a closed tube whose cross-section is an *elliptic umbilic* ( $D_{-4}$ ) catastrophe. The cross-section, shown in Fig. 2, is characterized by three cusps. A caustic ring is located near where the particles with the most angular momentum in a given inflow are at their distance of closest approach to the galactic center before falling back out. In section II, we gave estimates of the radii and the fold coefficients of the outer caustics, based upon the self-similar infall model. For the inner caustic rings, the curvature radii and fold coefficients depend on position on the surface of the ring caustic. We derived formulae for these quantities as a function of position (parametrized by  $\tau_1$ ) and of the five caustic ring parameters ( $a, b, u, \tau_0, s$ ). A great fraction of the surface of a caustic ring ( $0 < |\frac{\tau_1}{\tau_0}| < \frac{3}{4}$ ) is saddle-shaped and therefore has tangent directions along which the curvature of the surface vanishes. Finally, in section II, we derived the mass density profile near a cusp caustic.

Gravitational lensing was discussed in section III. In general, the shift in image position is the gradient of a potential whose 2-dim Laplacian is the column density. For an arbitrary

mass distribution, the procedure for calculating the shift involves two steps. First the matter density is integrated along the line of sight to obtain the matter density. Second, the potential is obtained by convoluting the column density with the 2-dim. Green's function. In the case of lensing by dark matter caustics, this procedure can be simplified: the shift is expressed directly as an integral over the parameter space of the dark matter flow forming the caustic. The relevant result is given in Eqs. (3.19) and (3.20) if the caustic has contrast in the two dimensions transverse to the line of sight, and in Eq. (3.25) if the caustic has contrast in only one of the dimensions transverse to the line of sight.

In section IV, we applied our formalism to the gravitational lensing by dark matter caustics in four specific cases. In the first three, the line of sight is tangent to a surface where a simple fold catastrophe is located. The three cases are distinguished by the curvature of the caustic surface at the tangent point in the direction of the line of sight: 1) the surface curves toward the side with two extra flows, 2) the surface curves away from the side with two extra flows, and 3) the surface has zero curvature. In the fourth case (4) studied, the line of sight is at a specific location close to a cusp catastrophe and parallel to the plane of the cusp. We found that each case has characteristic lensing signatures. In three of the cases (2, 3 and 4) there are multiple images and infinite magnification of point sources when their images merge. In case 1, there are no multiple images. Unfortunately, the effects are small even for dark matter caustic lenses at cosmological distances. The multiple images of a point source cannot be resolved with present instruments. Typical magnifications and image distortions are of order one % to a few %.

## VI. ACKNOWLEDGMENTS

We would like to thank Stuart D. Wick and Achim Kempf for stimulating discussions. This work was supported in part by the U.S. Department of Energy under grant DE-FG02-97ER41209, and by the National Science Foundation under grant PHY99-07949.

## REFERENCES

- [1] B. Paczynski, *Astrophys. J* **304** (1986) 1; C. Alcock et al., *Nature* **365** (1993) 621; E. Aubourg et al., *Nature* **365** (1993) 623; A. Udalski et al., *Acta Astron.* **43** (1993) 289.
- [2] R. Lynds and B. Petrosian, *Bull. Am. Astron. Soc.* **18** (1986) 1014; G. Soucail, B. Fort, Y. Mellier and J.-P. Picat, *Astron. Astroph. Lett.* **172** (1987) L14; J.A. Tyson, F. Valdes and R.A. Wenk, *Ap. J. Lett.* **349** (1990) L1; N. Kaiser and G. Squires, *Ap. J.* **404** (1993) 441.
- [3] P. Sikivie, *Phys. Lett.* **B432** (1998) 139.
- [4] P. Sikivie, *Phys. Rev.* **D60** (1999) 063501.
- [5] S. Tremaine, *MNRAS* **307** (1999) 877.
- [6] C. Hogan, astro-ph/9811290, to be published in *Ap.J.*
- [7] P. Sikivie and J. Ipser, *Phys. Lett.* **B291** (1992) 288.
- [8] P. Sikivie, astro-ph/0109296
- [9] D.F. Malin and D. Carter, *Nature* **285** (1980) 643.
- [10] L. Hernquist and P.J. Quinn, *Ap. J.* **312** (1987) 1.
- [11] P. Sikivie, I. Tkachev, Y. Wang, *Phys. Rev. Lett.* **75** (1995) 2911; *Phys. Rev.* **D56** (1997) 1863.
- [12] J.A. Filmore, P. Goldreich, *Ap. J.* **281** (1984) 1.
- [13] E. Bertschinger, *Ap. J. Suppl.* **58** (1985) 39.
- [14] A thorough account can be found in P. Schneider, J. Ehlers and E.E. Falco, *Gravitational Lenses*, Springer 1992.

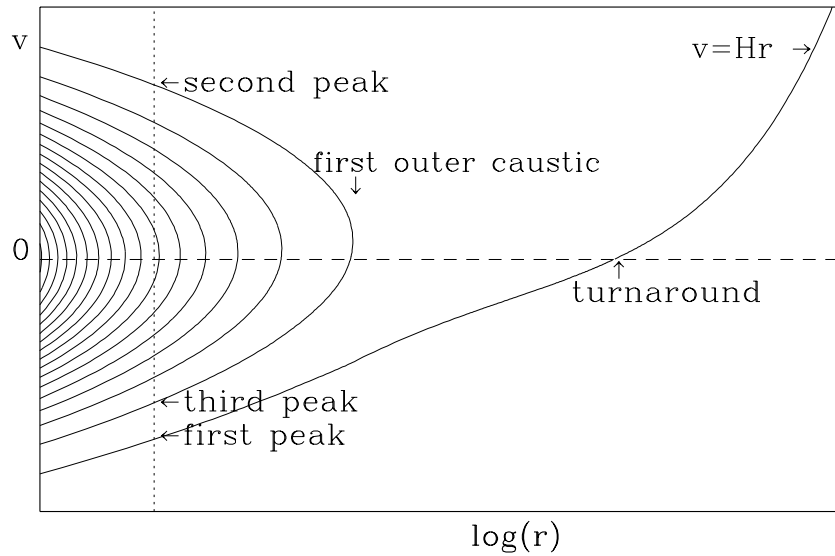


FIG. 1. A snapshot of the phase-space distribution of CDM particles in a galactic halo. For simplicity, spherical symmetry is assumed.  $r$  is galactocentric distance and  $v$  is radial velocity. The solid line indicates the location of the particles. The dotted line corresponds to the observer position. Each intersection of the solid and dotted lines corresponds to a CDM flow at the observer's location. "Turnaround" refers to the moments in a particle's history when it has zero radial velocity with respect to the galactic center. A "caustic" appears wherever the phase-space line folds back. Particles pile up and hence the density diverges there.

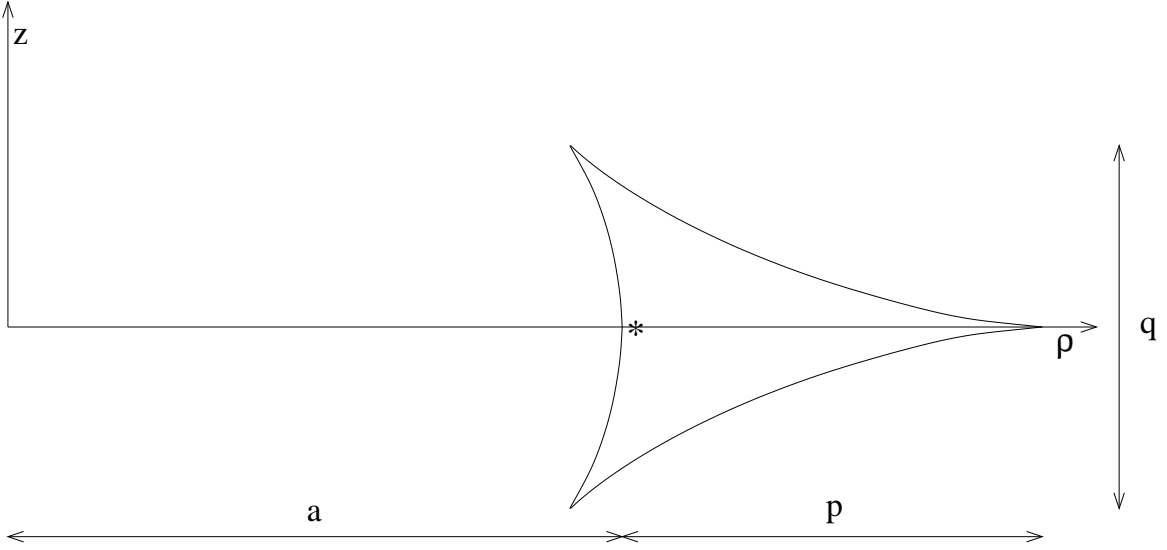


FIG. 2. Cross-section of a caustic ring in the case of axial and reflection symmetry.  $p$  and  $q$  are the transverse dimensions in the  $\hat{\rho}$  and  $\hat{z}$  directions respectively.  $a$  is the ring radius. The star indicates the sample location ( $\rho \simeq a, z = 0$ ) discussed in section II.B.1. For clarity, we took  $p, q \sim a$ . For actual caustic rings,  $p, q \ll a$ .

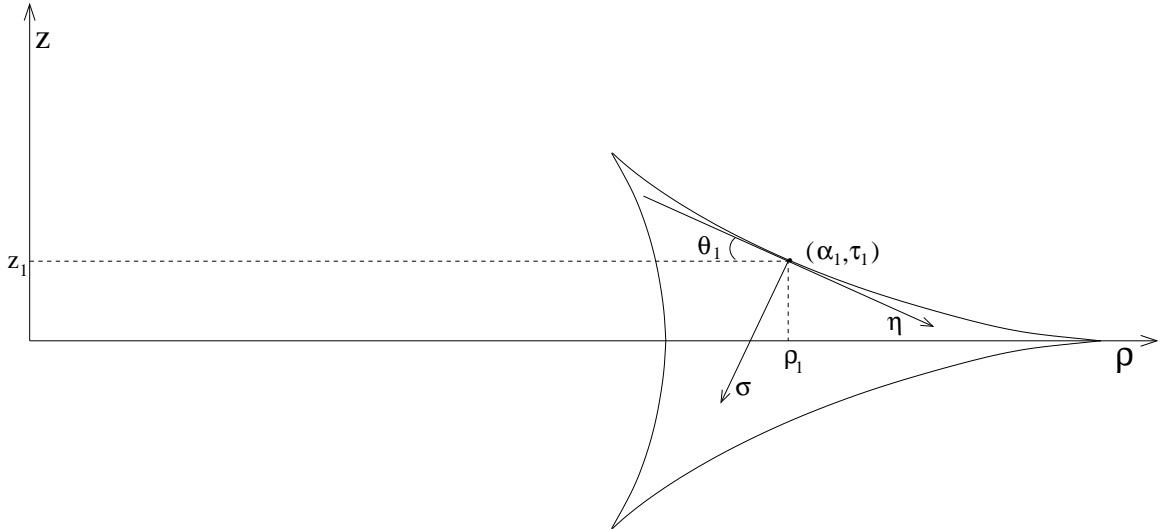


FIG. 3. An arbitrary point on the tricusp is labeled by  $\tau_1$  with  $\alpha_1 = \alpha_1(\tau_1)$ . Its physical coordinates are  $(\rho_1, z_1)$ . A new Cartesian coordinate system  $(\sigma, \eta)$  is defined there such that  $\hat{\sigma}$  is perpendicular to the caustic surface. It is rotated relative to the  $(\rho, z)$  coordinates by an angle  $\theta(\tau_1) + \frac{\pi}{2}$ .

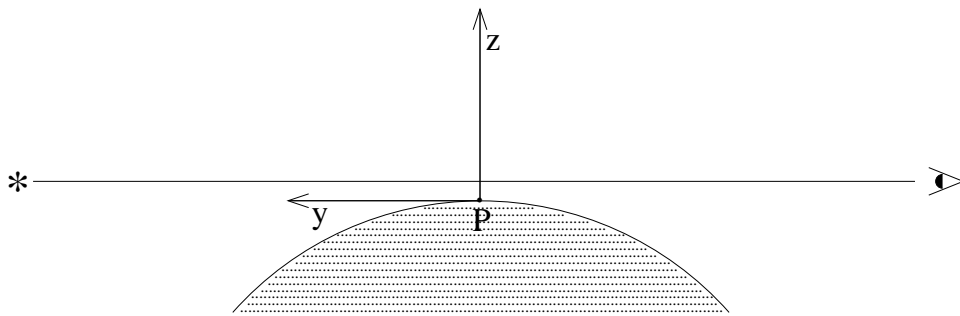


FIG. 4. Lensing by a concave fold. The arc is the intersection of the caustic surface with the plane containing the normal ( $\hat{z}$ ) to the surface and the line of sight ( $\hat{y}$ ). The shaded area indicates the side with the two extra flows.

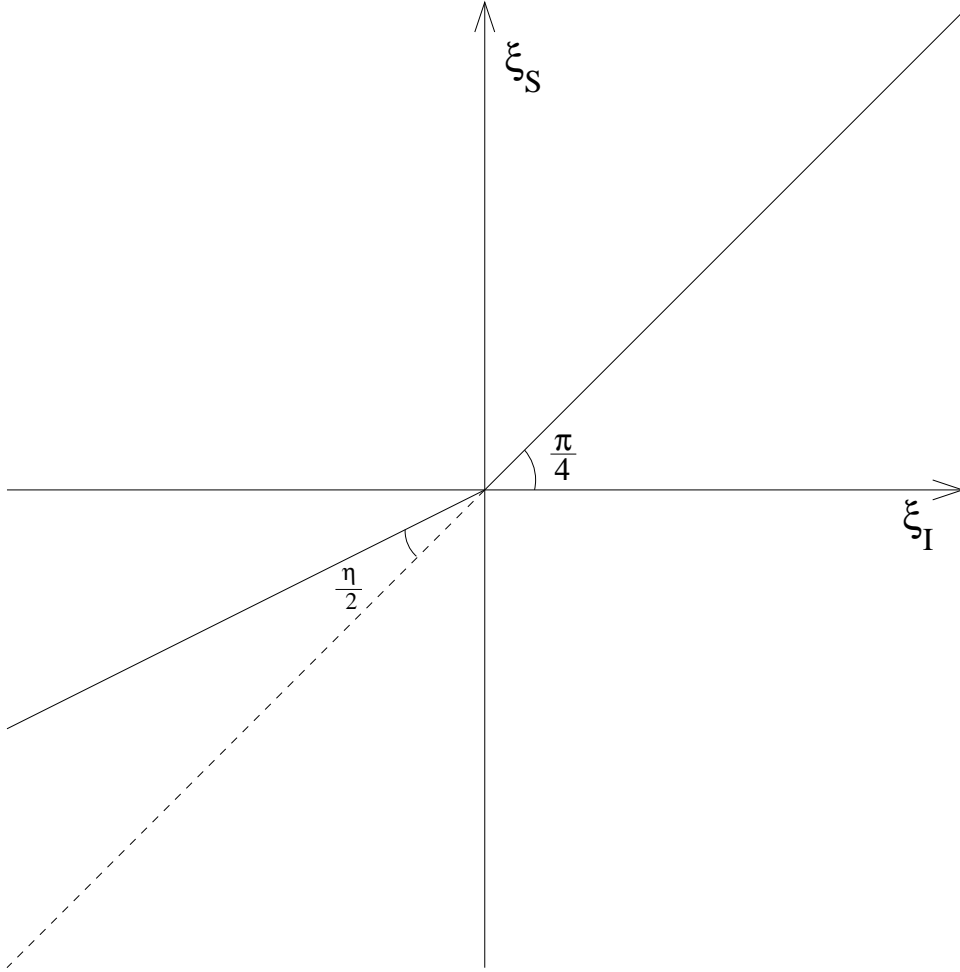


FIG. 5. Source position  $\xi_S$  as a function of image position  $\xi_I$  for lensing by a concave fold.  $\eta$  is given by Eq. (4.5) in terms of the fold coefficient and the curvature radius of the caustic surface. Estimates of  $\eta$  for the outer caustics of galactic halos are given in Eq. (4.9).

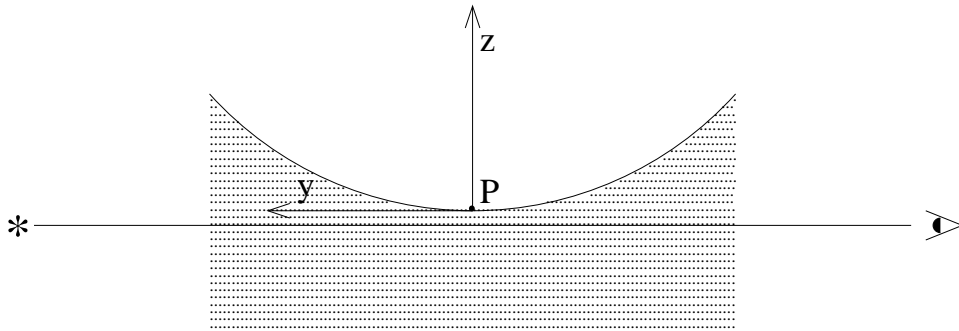


FIG. 6. Lensing by a convex fold. Same as Fig. 4 except that now the caustic surface curves away from the side with two extra flows.

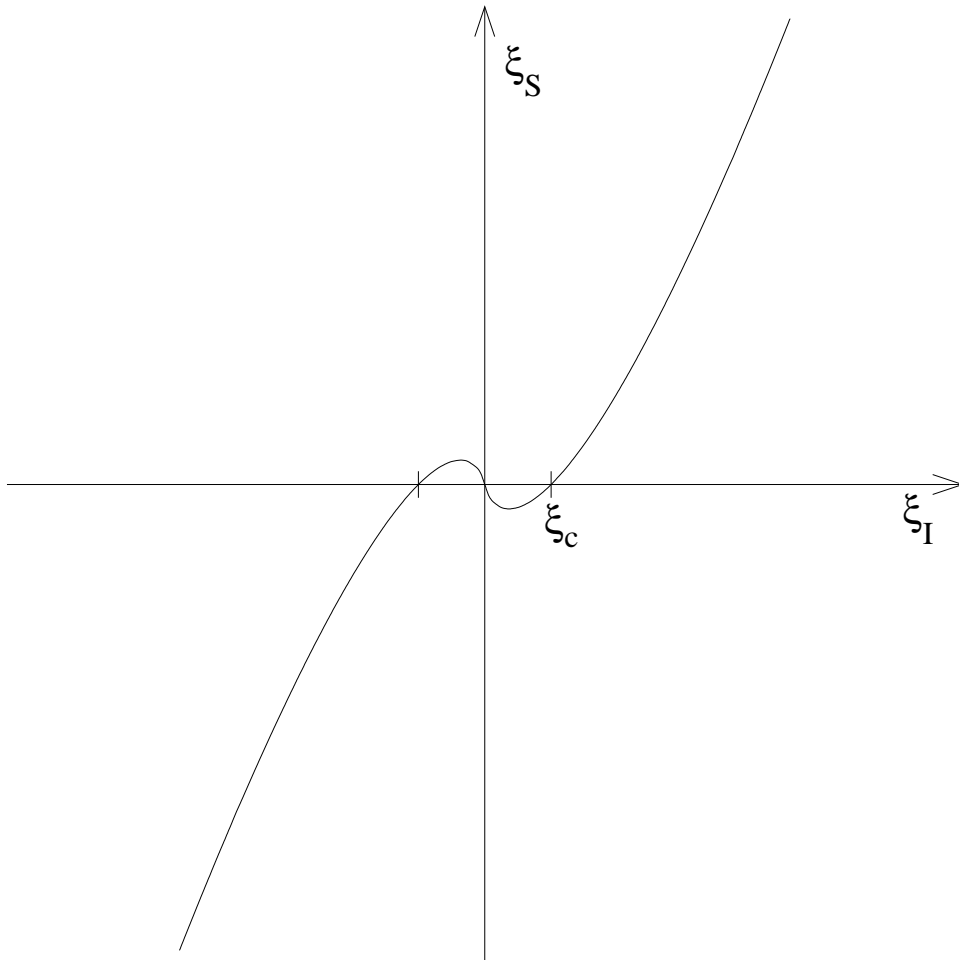


FIG. 7. Source position  $\xi_S$  as a function of image position  $\xi_I$  for lensing by a convex fold.  $\xi_c$  is given in Eq. (4.15).



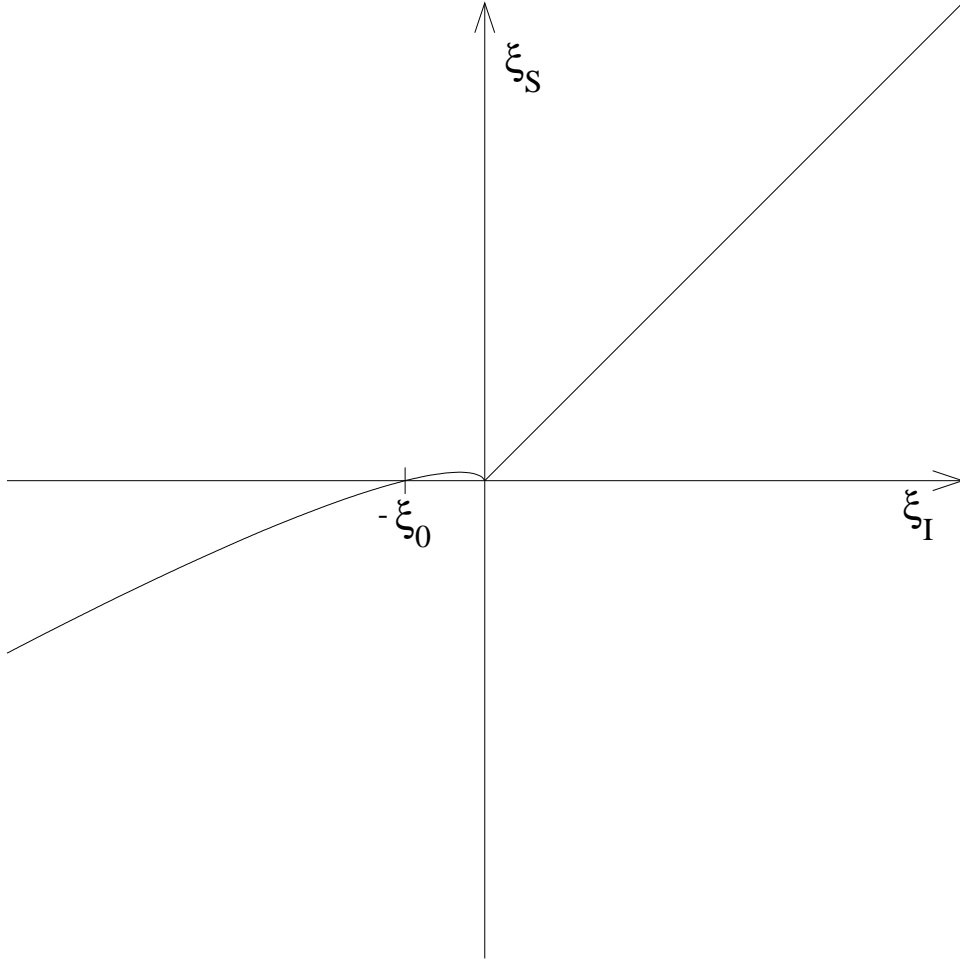
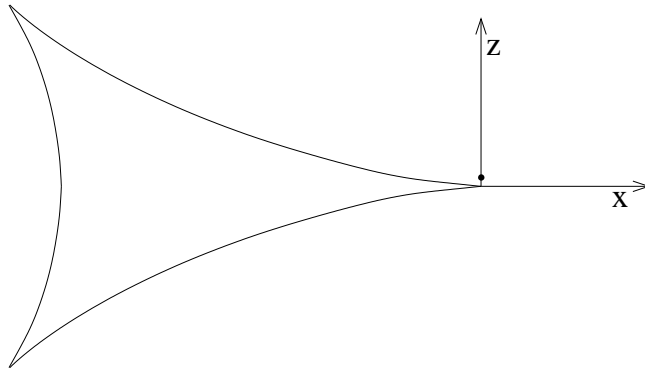


FIG. 8. Source position  $\xi_S$  as a function of image position  $\xi_I$  for lensing by a fold with zero curvature.  $\xi_0$  is given in Eq. (4.21).

a)



b)

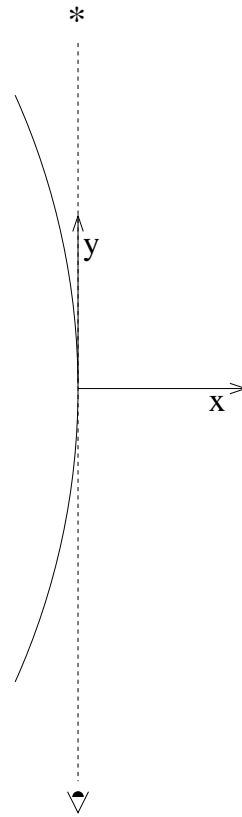


FIG. 9. Lensing by the caustic ring cusp at  $(z, \rho) = (0, \rho_0)$ , with line of sight parallel to the  $z = 0$  plane. We define  $x \equiv \rho - \rho_0$ . a) Side view in the direction of the line of sight. The latter is represented by the dot near  $x = z = 0$ . b) Top view. The curve is the location of the cusp in the  $z = 0$  plane.

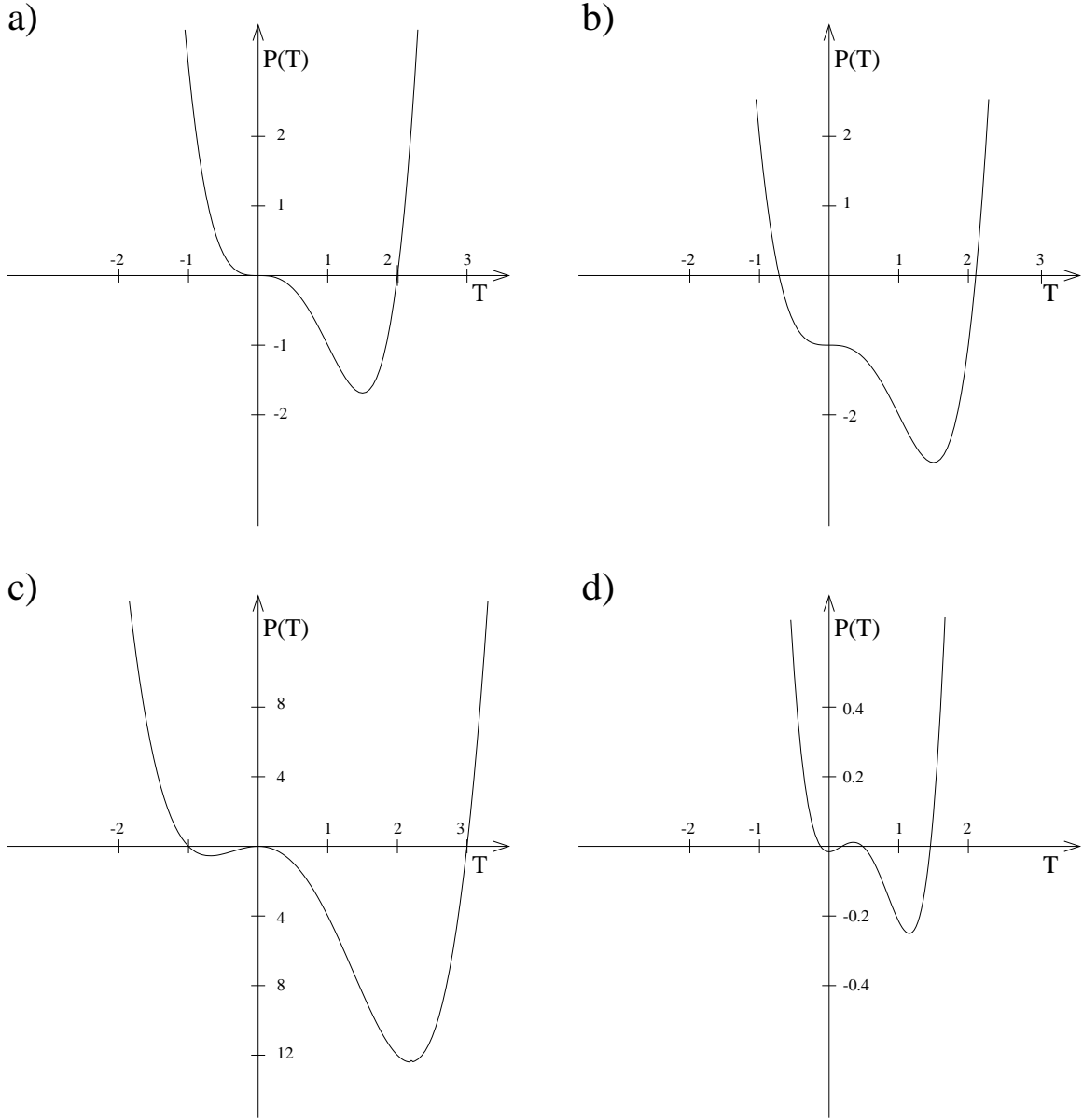


FIG. 10. Graphs of the quartic polynomial  $P(T) \equiv T^4 - \zeta(2T^3 + XT^2) - \frac{\zeta Z^2}{4}$  for  $\zeta = 1$  and  $(X, Z) = (0, 0), (0, 2), (1/3, 0)$  and  $(-1/3, 0)$ ; a) through d) respectively.

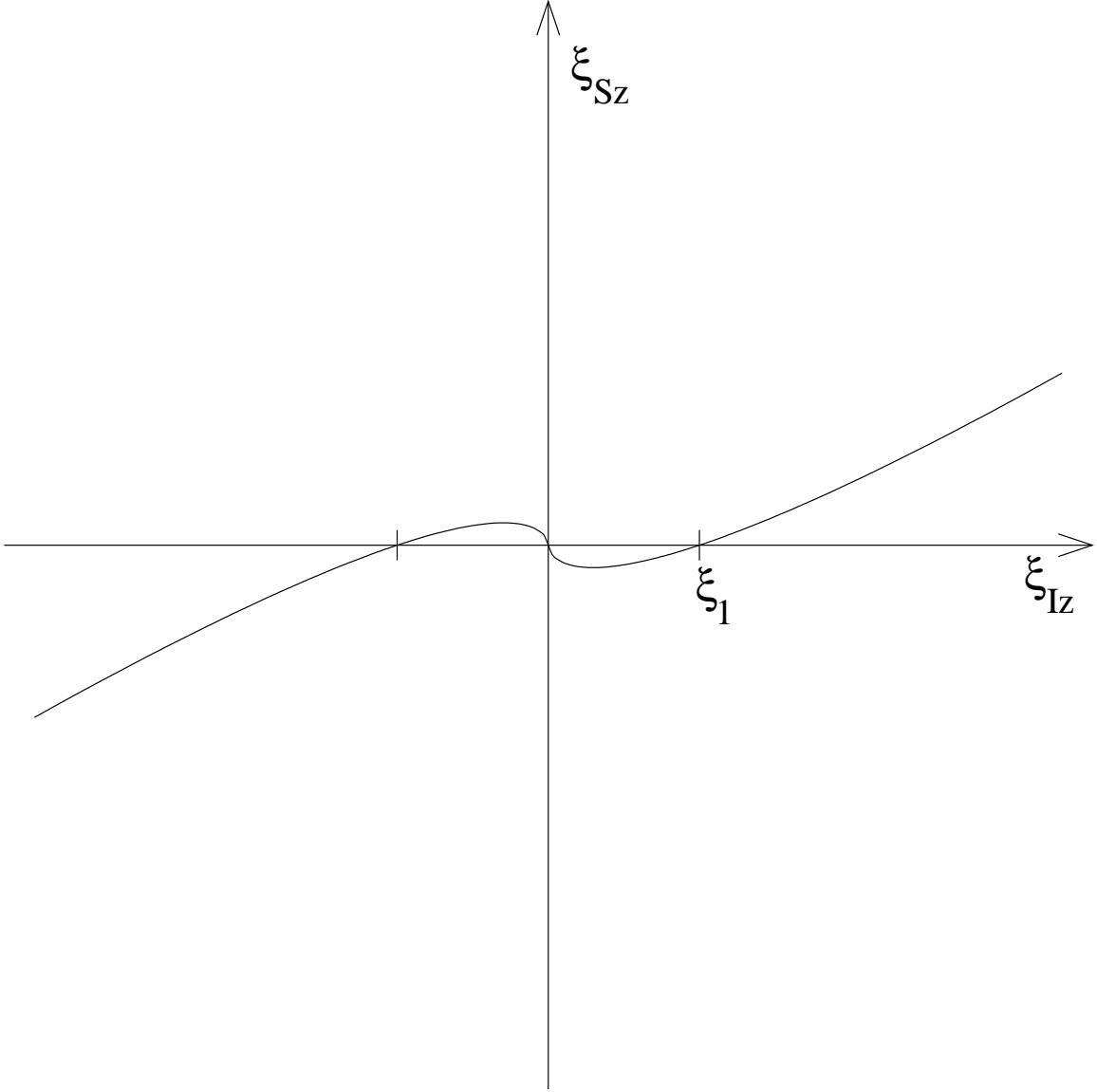


FIG. 11. Source position  $\xi_{Sz}$  as a function image position  $\xi_{Iz}$  for lensing by a cusp along the line of sight described in Fig. 9.  $\xi_1 \sim \eta''^3$  where  $\eta''$  is given by Eq. (4.36).